J. Fluid Mech. (1988), *vol.* 191, *pp.* 247–286
Printed in Great Britain

The planforms and onset of convection with a temperature-dependent viscosity

By DAVID B. WHITE
Schlumberger Cambridge Research, P.O. Box 153, Cambridge CB3 0HG, UK

(Received 11 May 1983 and in revised form 1 November 1987)

An experimental investigation was made of convection in a fluid with a strongly temperature-dependent viscosity. The determination of the critical Rayleigh number, R_c, using the appearance of convection to define onset, was complicated by the occurrence of subcritical instabilities initiated by horizontal temperature gradients at the side boundaries. The increase in R_c over the expected value was less than predicted by linear theory, probably owing to the effect of finite conductivity boundaries and the temperature dependence of other fluid properties.

The stability of various convective planforms was studied as a function of Rayleigh number, wavenumber and viscosity variation using controlled initial conditions to specify the wavenumber and pattern, Rayleigh numbers of up to 63000 and viscosity variations of up to 1000. In addition to the rolls and hexagons seen in constant- and weakly temperature-dependent-viscosity fluids, a new planform of squares was observed at large viscosity variations.

Experiments with viscosity variations of 50 and 1000 showed that hexagons and squares were stable at Rayleigh numbers less than 25000 over a limited range of wavenumbers, which was shifted to higher values with increasing viscosity variation. Temperature profiles through the layer revealed that this shift in wavenumber was associated with the development of a thick, stagnant, cold boundary layer which reduced the effective depth of the layer.

Experiments with a fixed wavenumber showed that rolls were unstable at all Rayleigh numbers for a viscosity contrast greater than 40, whereas squares did not become stable until the viscosity contrast exceeded 6. At low viscosity variations and high Rayleigh numbers rolls became unstable to a bimodal pattern, but at high viscosity variations and a Rayleigh number of 25000 squares broke down into the spoke pattern, a convective flow not observed until Rayleigh numbers of around 100000 in a constant-viscosity fluid.

1. Introduction

To understand convection in a fluid with a temperature-dependent viscosity we need to study the onset of convection, the planform of the convective motions and their scale, the thermal structure and the heat flux transported through the layer. Such studies are important in furthering our understanding of convection in the Earth's mantle and its effect upon the scale of plate motions and heat flow, as the deformation in the mantle is known to be a strong function of temperature. The properties of convection in a constant-viscosity fluid are now fairly well understood, and from this basis we can determine the modifications to the behaviour of the flow due to a variable viscosity.

There have been many studies, both theoretical and experimental, to determine

the planform of convection in a constant-viscosity fluid heated from below. Among the key papers is Busse's (1967*a*) work on the stability of planforms for convection up to 14 R_c, where R_c is the critical Rayleigh number, using numerical methods which found that two-dimensional rolls were unstable to infinitesimal three-dimensional disturbances except within a closed region commonly called the 'Busse balloon'. Above a Rayleigh number of 22600 all two-dimensional rolls we unstable and a transition to three-dimensional flow occurred. Busse & Whitehead (1971), using techniques developed by Chen & Whitehead (1968), performed laboratory experiments showing very good agreement with the theoretical predictions.

Many experiments have been performed in the past to measure heat flux as a function of the Rayleigh number, but with a variable viscosity there is no unique viscosity with which to define the Rayleigh number. Booker (1976) made heat-flux measurements with convection in Polybutene oil and found that, by defining the Rayleigh number using the fluid properties at the mean of the boundary temperatures, the Nusselt number–Rayleigh number relationship was very similar to that for a constant-viscosity fluid. Wray (1978) and Richard, Nataf & Daley (1983), using Lyle's Golden Syrup, reached the same conclusion, which suggests the following definition of the Rayleigh number for the experiments:

$$R = \frac{g\alpha\Delta T d^3}{\kappa\nu},$$

where g is the acceleration due to gravity, α is the coefficient of thermal expansion, ΔT is the temperature drop across the layer, d is the layer depth, κ is the thermal diffusivity, and ν is the kinematic viscosity at the mean of the boundary temperatures.

Palm (1960) showed that a variable-viscosity fluid could produce a hexagonal planform, and Busse's (1967*b*) analysis of a weakly temperature-dependent viscosity predicted the existence of subcritical, finite-amplitude hexagons and hysteresis in their transition to rolls at a higher Rayleigh number. This was experimentally verified by Somerscales & Dougherty (1970) and Hoard Robertson & Acrivos (1970). Wray (1978) found irregular polygons in all his variable-viscosity flows with Rayleigh numbers below 20000. Richter (1978) showed that the stability of rolls with viscosity variations between 2 and 6 were very similar to those for a uniform-viscosity fluid, the only differences being a reduction in the Rayleigh number, R_B, at which the transition to bimodal flow occurred and the existence of stable hexagons at low Rayleigh numbers and large viscosity variations. He found no new planforms. In some recent finite-amplitude work Oliver & Booker (1983) observed hexagons and a new planform of squares. However, their determination of the stability of different planforms was affected by the circular geometry of their apparatus and the spatial irregularity of the convection cells as no regular pattern could be induced.

Using linear theory Wray (1978) showed that, for a fluid with an exponential variation, R_c should initially increase with increasing viscosity variation. Stengel, Oliver & Booker (1982) experimentally determined the onset of convection in a variable-viscosity fluid by measuring the heat flux and found an increase in R_c with increasing viscosity variation. The infinitesimal amplitude state was found to be not steady, and convection grew to finite amplitude at R_c as seen by a jump in the Nusselt number. The thermal structure and heat flux of convective flows with viscosity variations up to 10^5 have been studied by Richter *et al.* (1983), whose work forms an important complimentary study to this paper. Their temperature profiles show the development of a thick stagnant boundary layer, a result confirmed in §7.

Additionally their determination of the Nusselt number for Rayleigh numbers near R_c in flows viscosity variations of 3×10^3 and $\sim 10^5$, revealed the existence of subcritical, finite-amplitude convection.

In experimental design, the requirements for accurate measurements of heat flux make visualization of the flow very difficult as the layer can only be observed from the edge. Conversely, if visualization is simple, then heat-flux measurements cannot be accurately made. In this paper the latter route has been taken and experimental apparatus and techniques similar to Busse & Whitehead (1971) employed, so that various planforms can be initiated and their stability determined.

The initial experiments with random initial conditions described in §3 showed that the experimental determination of R_c is complicated by the presence of horizontal temperature gradients which drive a flow that resonates with the subcritical state and starts convection below R_c. If this effect is accounted for then R_c initially increased with increasing viscosity variation but not as rapidly as predicted by linear theory. The planform experiments in §§5 and 6 showed that squares are a stable planform with a stability region similar to the Busse balloon for rolls, although it is increasingly shifted to larger wavenumber, k, with increasing viscosity variation. Hexagons were stable within a smaller area of (R, k)-space but again shifted to larger k with increasing viscosity variation. In §8 experiments varying the viscosity with a fixed k revealed squares to be unstable at all Rayleigh numbers below a viscosity variation of 6.

2. The apparatus and procedure

The apparatus allows the establishment of controlled initial conditions and the subsequent observation of the convective planform. The fluid layer was bounded above and below by 6 mm float-glass manifolds, each consisting of two parallel glass plates separated by a 6 mm gap forming a water channel (figure 1). The temperatures of the horizontal boundaries of the fluid layer were set by the flow of thermostated water through these channels. The layer depth was fixed by removable spacers machined to 4×10^{-5} mm and depths of 5 and 6 cm were employed compared with the 1 m × 95 cm horizontal dimension of the tank. Power was supplied to the hot-water bath by a 1500 W thermistor-controlled heater with an additional back-up heater with a variable power of 0–1000 W. Two different refrigeration units were available with dissipation rates of 1500 or 2500 W.

The apparatus was levelled to 1 in 10^4. As any variation in depth causes a change in the Rayleigh number, the bending of the glass plates bounding the layer was minimized by maintaining the correct hydrostatic head to within 1 mm. The water-bath temperatures were kept constant to within ± 0.02 °C during the 24 h of a typical experiment. The flow in the two manifolds was in opposite directions in order to maintain a constant temperature difference across the layer. The temperature difference between the inlet and outlet was usually less than 0.4 °C, compared with a typical vertical temperature difference of 40 °C, but in extreme cases it was as large as 0.7 °C. The Rayleigh numbers quoted were calculated using the fluid properties at the mean of the inlet and outlet water temperatures. A higher flow rate of water would have reduced the horizontal temperature gradient but the differential pressure across the channel would produce greater bending of the glass.

The water temperatures were measured using thermistors in the inlets and outlets of the manifolds which were calibrated to 0.01 °C against the thermometer that was later used in the viscosity measurements of the syrup. To find the boundary

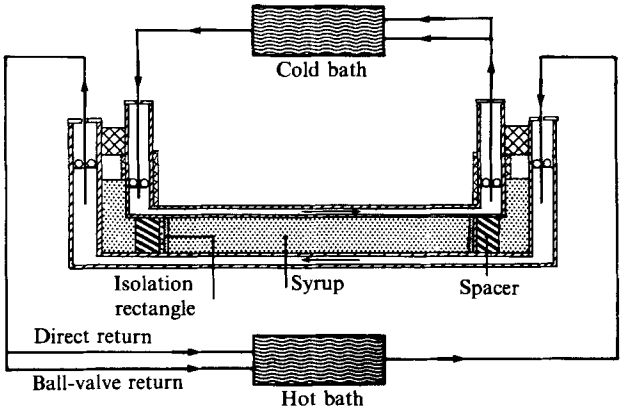

FIGURE 1. A schematic diagram of the apparatus. The fluid layer was heated from below and cooled from above by water supplied to the two manifolds from the constant-temperature water baths. The return flow was trimmed by the ball valve to exactly equal the input and thus maintain the water levels constant. The water channels were covered with polypropylene balls to reduce evaporation.

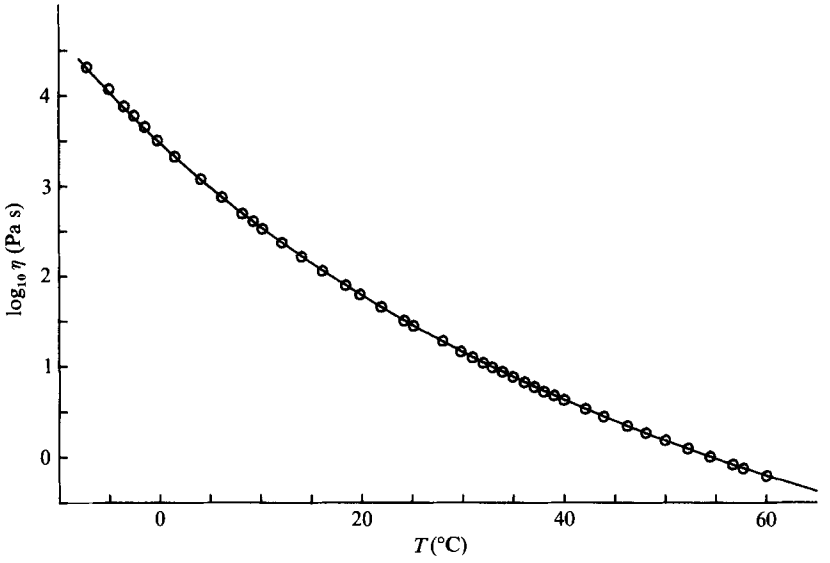

FIGURE 2. The viscosity of Lyle's Golden Syrup as a function of temperature. The curve was calculated from expression (1).

temperatures of the fluid from the water-bath temperatures a correction had to be made for the temperature drop across the glass. This correction was calculated using an experimentally determined Nusselt-number relationship for syrup, $Nu = 0.1775\ R^{0.2775}$, obtained by Wray (1978). The largest correction was about 10% of the temperature difference between the baths. The viscosity variation, ν_{max}/ν_{min}, was defined as the ratio of the viscosity at the calculated cold boundary temperature to that at the hot boundary temperature. The boundary temperatures were measured, in the conductive state, using a set of six thermistors attached to each boundary and agreed to within 0.5% of the calculated values. When the fluid is convecting the error in the calculated temperature difference across the glass will be mainly from errors

in the Nusselt-number relationship and amount to a few per cent. The viscosity of the syrup was known to better than 1% but there are larger uncertainties in the values of α and C_p, the specific heat capacity, which combine to give a possible error of about 10% in the absolute value of the Rayleigh number. The relative values of the Rayleigh number are accurate to about 5%.

To avoid possible edge effects due to non-uniform temperature gradients, a region of fluid was isolated from the edges by an 80×85 cm wall of Perspex 0.5 cm thick, its conductivity being similar to that of syrup. This isolation rectangle had foam on both edges which compressed to give a good fit between the upper and lower manifolds with a depth set by the accurately machined spacers.

Lyle's Golden Syrup has a strongly temperature-dependent Newtonian viscosity (figure 2). The viscosity was determined, to an accuracy of better than 1%, between $-10°$ and 65 °C using a falling-ball viscometer with corrections for a finite-sized cylinder. Details of the viscosity are from White (1981) and the other physical properties, taken from Wray (1978), are as follows:

$$\alpha = 4.33 \times 10^{-4}\ ^\circ\mathrm{C}^{-1} \text{ (accurate to } \sim 1\%);$$

$$\rho_{20} = 1438\ \mathrm{kg\ m^{-3}} \text{ (accurate to four significant figures)};$$

$$C_p = 2.02 \times 10^3\ \mathrm{J\ kg^{-1}\ ^\circ C^{-1}} \text{ (accurate to a few \%)};$$

$$K = 0.3158 + 1.8431 \times 10^{-3} T\ \mathrm{W\ m^{-1}\ ^\circ C};$$

where T is the temperature in °C.

The thermal conductivity K was measured at the Ministry of Defence, Explosives Research and Development Establishment, using an industrial co-axial cylinder with an accuracy of 2%. However, measurements by Richter *et al* (1983) suggests that this value may be in error and that it should be $0.353 + 1.0 \times 10^{-5} T$ W m^{-1} °C^{-1}. The Rayleigh numbers quoted in this paper use the former value. The viscosity measurements were fitted to a curve of the form

$$\eta = \eta_0 \exp\left(\frac{1}{A + BT - CT^2}\right) \mathrm{Pa\ s}. \tag{1}$$

A typical curve had coefficients $\eta_0 = 5.37996 \times 10^{-8}$ Pa s; $A = 4.04028 \times 10^{-2}$; $B = 3.93566 \times 10^{-4}\ T^{-1}$; $C = 7.08166 \times 10^{-7}\ T^{-2}$.

The viscosity of each batch of syrup used was checked, and all were within 5% of each other. During viscosity measurements it was observed that the syrup began to degrade above 60 °C. Although this degradation made no difference to the viscosity, it was used as an upper limit for the hot boundary temperature in the experiments. Another problem occurred after a few months when sugar crystals formed and were concentrated under rising regions to produce very dark spots on some of the photographs. The syrup was then changed, although the viscosity of a sample of syrup that had been in the tank for four months was found to be within 0.3% of its original value. The Prandtl number, ν/κ, is around 10^5 for the mean temperatures used, but varies between 2×10^7 at the cold boundary and 5×10^3 at the hot boundary.

Experiments were carried out with a fixed viscosity variation at different Rayleigh numbers. This fixed viscosity variation was achieved by varying the mean temperature, and thus the mean viscosity of the layer, with a small alteration in ΔT to allow for the fact that the temperature–viscosity curve is super-exponential. This procedure is in contrast with the methods of Richter (1978), who fixed the mean

temperature and altered the Rayleigh number by changing ΔT, thus also changing the viscosity variation.

The convection pattern was visualized using the standard shadowgraph technique. Light from a 250 W slide projector was passed though a 6 mm hole then bounced off one large mirror, through the layer, off a second mirror and on to a frosted screen with a total light path of about 4 m. Light passing through a cold, sinking region is focused, producing a bright line on the screen from a sinking sheet or a bright spot from a sinking plume. Light traversing a hot, rising region is defocused to produce dark lines or spots on the screen. The resulting picture is a pattern of light and dark lines that may intersect, as the shadowgraph is a complicated vertical integration of the temperature field of the layer.

To induce convection with the desired pattern the method of Chen & Whitehead (1968) was used. The layer was held in a subcritical condition for about 15 h ($d^2/\kappa \sim 7$ h) and then a mask of the desired pattern and wavelength was placed over the layer. Light from eight 300 W heat lamps was reflected off the top mirror, down through the mask for a further hour, producing periodic temperature perturbations of the desired pattern in the fluid. The water-bath temperatures were then changed at equal rates of 0.2 °C/min until their final values were achieved. It is important to maintain the mean temperature of the layer constant with uniform heating and cooling as any asymmetric temperature profile specifically favours hexagonal patterns (Krishnamurti 1968). Although the temperature perturbations produced by the heat lamps are small, ~ 0.05 °C, the fluid starts to convect with the same pattern as the motions forced by the induced horizontal temperature gradients. Thus the initial pattern of rising regions is the same as the pattern of holes in the mask. Once convection appeared the heat lamps and mask removed and the convective planform was observed to determine its stability.

3. The onset of convection

3.1. *Numerical results*

The infinite-Prandtl-number and Boussinesq approximations were made in a numerical scheme, using linear theory, to calculate the critical Rayleigh number for an exponential and super-exponential viscosity variation. The latter was modelled on the viscosity–temperature relationship for Lyle's Golden Syrup. The method involved a propagator matrix technique and full details are given by White (1981).

A plot of R_c versus the viscosity variation for an exponential fluid, figure 3, initially shows a rise in R_c, as the viscosity variation is increased, until it reaches a peak value at $\nu_{max}/\nu_{min} \approx 1000$ after which it drops rapidly. The super-exponential viscosity function for Golden Syrup assumed a mean temperature of 20 °C and produces a larger increase in R_c at a given viscosity variation and reaches a peak value at $\nu_{max}/\nu_{min} \approx 3000$. Including the temperature dependence of the thermal conductivity of syrup, in addition to the viscosity, results in a larger increase in R_c. For both exponential and syrup-type viscosities the critical wavenumber drops very slightly as the viscosity variation is increased and then rises sharply for $B(= \ln(\nu_{max}/\nu_{min}))$. greater than 4 (figure 4).

Stengel *et al.* (1982) examined the onset of convection in cosine-, exponential- and super-exponential-viscosity fluids. Their results agree exactly with those calculated by White (1981) apart from their super-exponential function, tailored to fit the viscosity variation of glycerine, where the results agree qualitatively with those for

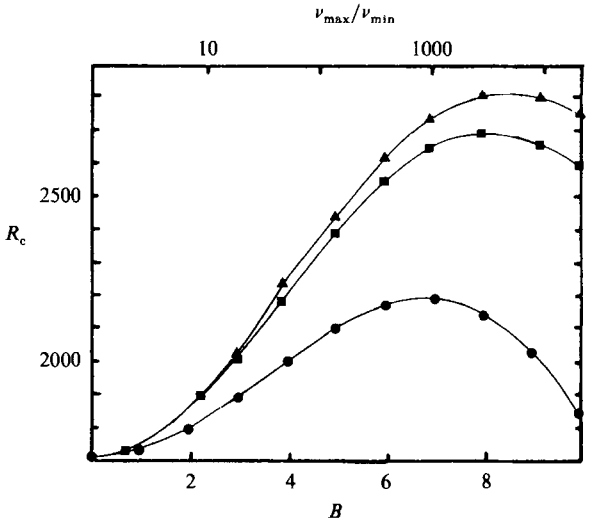

FIGURE 3. A plot of R_c versus $B(=\ln(\nu_{max}/\nu_{min}))$ for: ●, an exponential-viscosity fluid; ■, Golden Syrup; ▲, Golden Syrup, including the effects of a variable thermal conductivity.

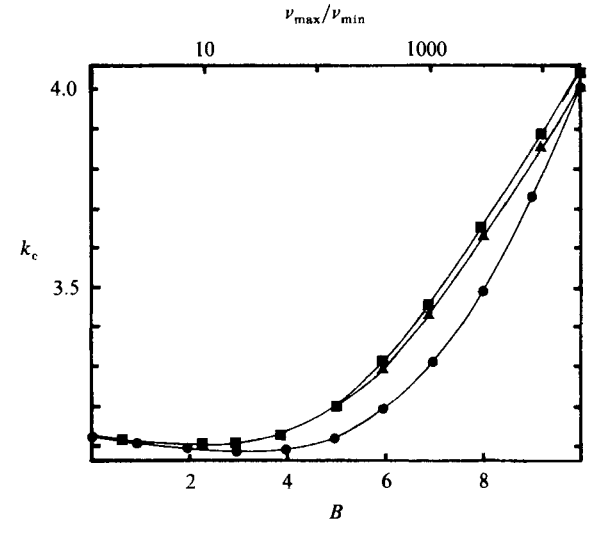

FIGURE 4. A plot of k_c versus $B(=\ln(\nu_{max}/\nu_{min}))$ for: ●, an exponential-viscosity fluid; ■, Golden Syrup; ▲, Golden Syrup, including the effects of a variable thermal conductivity.

syrup. The peak value of R_c for glycerine was higher, and occurred at a larger B than that for the exponential fluid. In addition they found that the inclusion of a temperature-dependent coefficient of expansion, α, and specific heat, C_p, in the glycerine function produced a reduction in R_c to below the value with constant α and C_p. The critical-Rayleigh-number curve for the syrup is similar to that found by Richter *et al.* (1983) who used a different approach to find R_c, involving a Green function and assuming a fixed bottom temperature of 80 °C.

The predicted increase of R_c for convection in syrup with a moderate viscosity variation is sufficiently large that it could be detected in the laboratory. Experiments were then carried out using visual observations to determine onset.

3.2. *Experimental results*

The onset of convection is best determined by measuring the heat flux though the layer to detect a change in the Nusselt number as convection starts. With the apparatus described above this measurement was not possible, so the criterion used was the appearance of a convection pattern. Initially both water baths were set at the mean temperature of the planned final state for 24 h to remove any temperature perturbations due to the previous pattern. The water-bath temperatures were then set to their final values and convection was allowed to develop from any random temperature perturbations present in the layer. The time taken for a convection pattern to appear and fill the tank was measured from when the water baths reached their final temperatures. Experiments were carried out at Rayleigh numbers in the range 1600–2500 and at a fixed viscosity variation of 50. At the lowest Rayleigh numbers investigated the first instability observed was not hexagonal. Figure 5 shows the development of convection with an initial Rayleigh number of 1690, which is below R_c calculated for a viscosity variation of 50 with the same mean temperature as the experiment. A convection roll is seen to have formed, at the bottom edge of the screen, which subsequently broke up into hexagons and a new roll formed farther out from the edge. The new roll also broke down into hexagons and again another roll formed farther out. The process was repeated until the whole layer was covered with hexagons. The evolution of the pattern was very slow so the Rayleigh number was increased for the last three pictures to reduce the observation time. The final pattern of uniform hexagons had a wavenumber, $k = 4\pi d/\sqrt{3}\lambda$, of 2.78, where λ is the separation of adjacent rising regions and d is the depth of the layer, smaller than the calculated critical wavenumber of 3.12. The initial roll from which the hexagons evolved had a wavenumber of 3.0 and lines through the centres of adjacent rows of hexagons retained this original spacing.

At a Rayleigh number of 2200 the pattern evolved in a different manner. As before the first observed instability was a roll which transformed into hexagons and the convection pattern propagated inwards from the bottom edge. Then, before half the screen was filled in the previous manner, convection appeared simultaneously over the rest of the layer. At still higher Rayleigh numbers the rolls and hexagons had only propagated a small distance in from the edge before a random polygonal pattern appeared all over the remainder of the tank (figure 6).

A plot of the inverse of the time taken to fill the layer with a convection pattern versus the Rayleigh number reveals two distinct trends (figure 7). The appearance of convection in runs with Rayleigh numbers less than 2100 (line 1) was due solely to the behaviour observed in figure 5, whereas the time taken for runs on line 2 was controlled by the behaviour illustrated in figure 6. The intersection of the two lines corresponds to a change in the nature of the growth of the convection pattern. The data points in experiments with very slow growth rates were obtained by observing the propagation of the rolls over several days and then extrapolating for the time that would be required to fill the layer.

The measurement of a critical Rayleigh number from figure 7 presents a problem. Convective motions, observed at a Rayleigh number as low as 1670, were initially in the form of a roll whereas the expected behaviour, the simultaneous appearance of polygons all over the screen, was observed for runs on line 2. At R_c in a constant-viscosity fluid the growth rate of the convective motion, σ, is proportional to $(R–R_c)$ which is reflected in the linearity of the points on line 2. Taking the intercept of line 2 on the y-axis where $1/t = 0$, i.e. zero growth rate, should give R_c. The value

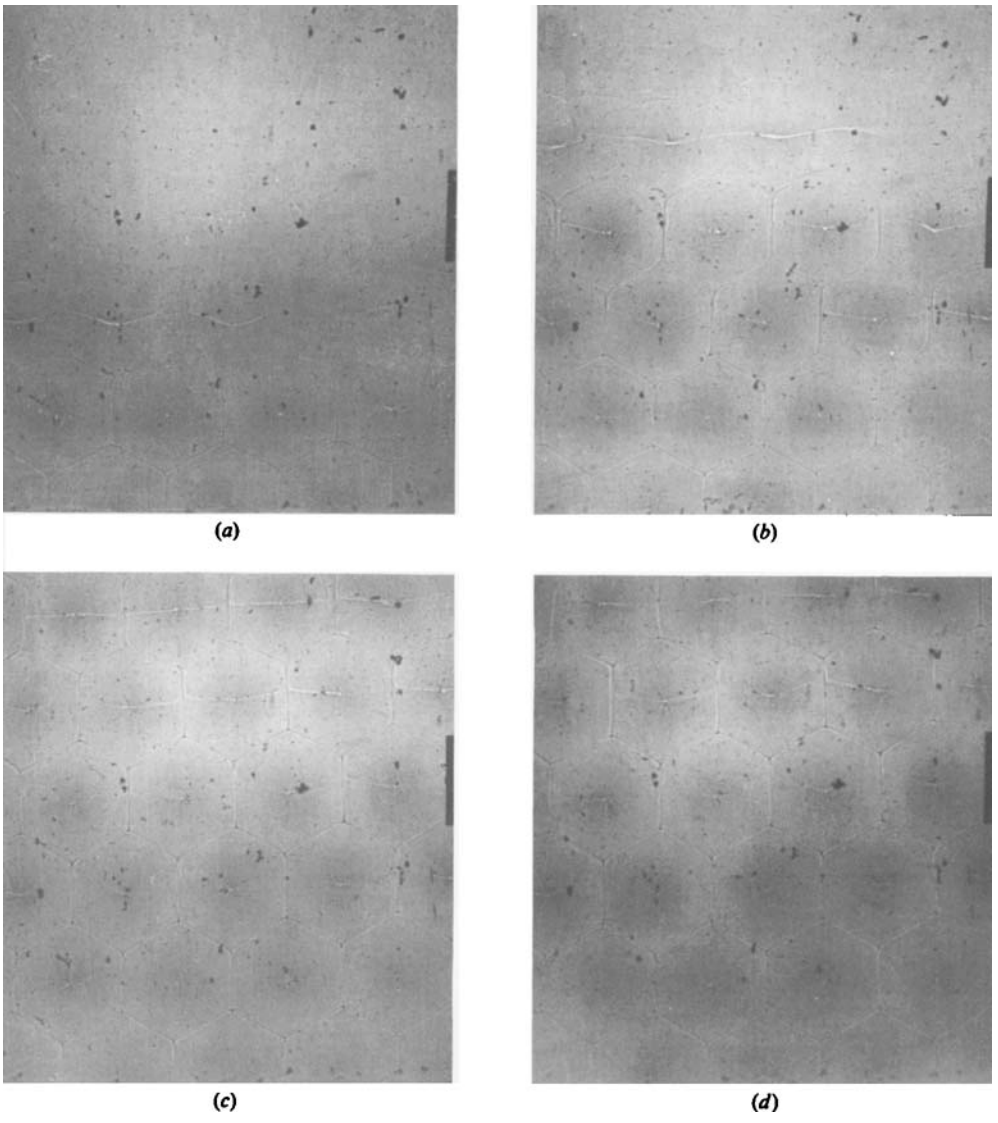

FIGURE 5. The appearance of convection from random initial conditions at a viscosity variation of 50. The marker was 10 cm long, twice the layer depth. (*a*) $R = 1690$, after 78 h another roll had formed farther out; (*b*) $R = 1780$ after 126 h; (*c*) $R = 1780$ after 149; (*d*) $R = 1780$ after 169 h.

obtained by this method is 1940, which is $\approx 14\%$ less than the calculated critical value of 2200 for a syrup-type viscosity with a variable thermal conductivity, but is greater than R_c for a constant-viscosity fluid. The calculated values of R_c are probably too large as the effect of the finite conductivity of the boundaries and the temperature dependence of C_p and α were not included. Richter *et al* (1983) studied the Nusselt number–Rayleigh number relationship for convection near critical in an experiment with a viscosity variation of 3000 and found that the measured value of R_c was 35% lower than that predicted by linear theory.

An explanation for the observations above can be given if we consider the occurrence of the subcritical instabilities predicted by Busse (1967*b*). No convection occurs when the Rayleigh number is increased until R_c is reached, when the amplitude

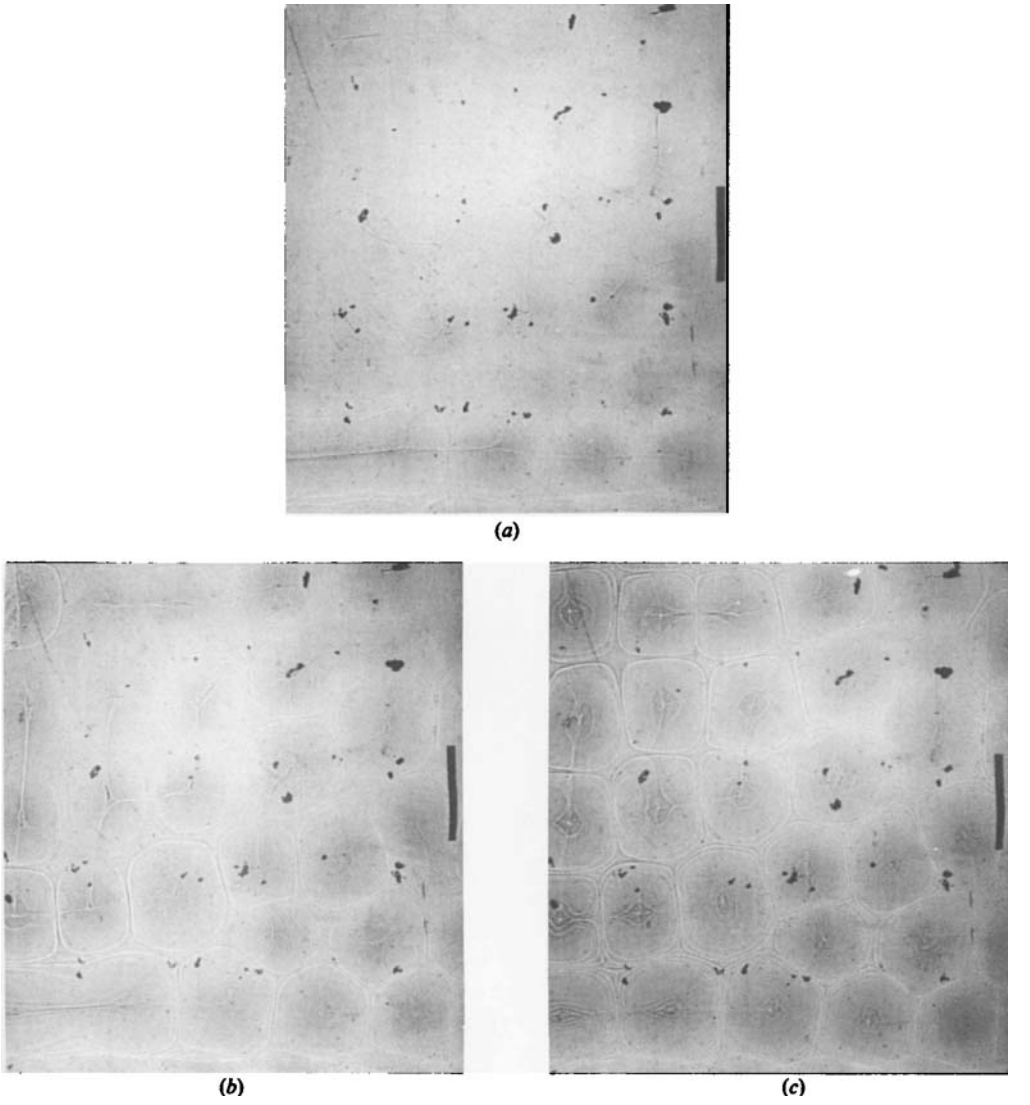

FIGURE 6. The appearance of convection from random initial conditions at a Rayleigh number of 2220 and viscosity variation of 50. After: (*a*) 328 min; (*b*) 452 min; (*d*) 576 min. The marker was twice the fluid depth.

grows to a finite value (figure 8). As the Rayleigh number is reduced convection will persist at finite amplitude until R_D is reached, with a corresponding minimum amplitude E_D, when it ceases.

If we now consider the existence of a boundary roll with an amplitude greater than E_D, then provided the Rayleigh number is above R_D, the boundary roll can resonate with the finite-amplitude convective state. At this Rayleigh number hexagons are the only stable finite-amplitude convection in a fluid with variable viscosity, so the roll breaks down into hexagons. The enhanced heat flux through the region in which convection is occurring will change the temperature at the boundaries owing to the finite conductivity of the glass. This change in temperature gives rise to further horizontal temperature gradient which aid the production of another boundary roll

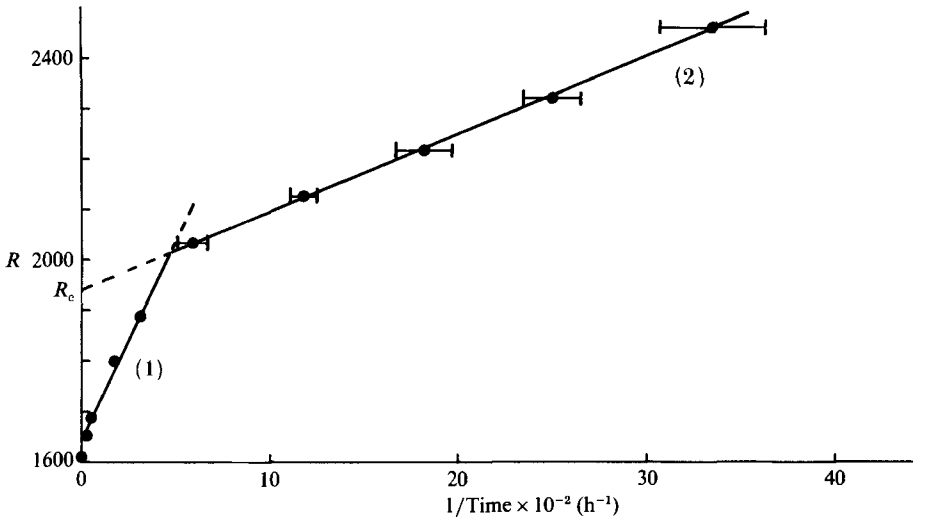

FIGURE 7. The inverse of the time taken for a convection pattern to fill the layer, in experiments with a viscosity variation of 50, versus the Rayleigh number. The appearance of convection in runs on line 1 was characterized by the propagation of rolls and hexagons, that on line 2 by the simultaneous appearance of polygons.

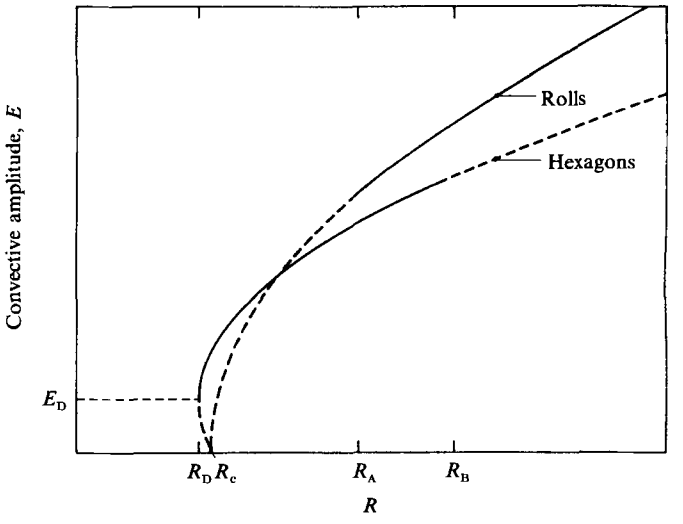

FIGURE 8. Qualitative sketch for the dependence of the amplitude of convection on the Rayleigh number for rolls and hexagons. Solid lines represent stable convection and dashed lines are for unstable convection. As the Rayleigh number is increased from zero, convection will start at R_c in the form of hexagons. These remain stable until R_B, when they transform into rolls. When decreasing the Rayleigh number from above, R_B rolls are stable until R_A, when they break down into hexagons. These hexagons persist below R_c until R_D is reached and convection ceases. (From Busse 1967*a*.)

farther out into the fluid. If the Rayleigh number is below R_D then no subcritical instability is possible and the boundary roll remains confined to the very edge. The intercept of line 1 with $1/t = 0$ will give the value of R_D. From figure 7, $R_D = 1640$ at a viscosity variation of 50. Richter *et al.* (1983) found R_D to be 1350 in an experiment using syrup at a viscosity variation of 3000.

For Rayleigh numbers greater than R_c the boundary rolls will still grow and resonate with the 'normal' convection. The time taken to fill the screen with a convective pattern is governed by the growth rate of the convective instability. From figure 7 we see that the growth rate of both types of convective instability is linear, but that of the normal convection increases more rapidly with increasing Rayleigh number than that of the boundary rolls.

3.3. *The onset of convection with controlled initial conditions*

The horizontal temperature gradients at the sidewalls represent uncontrolled perturbations which appear to initiate subcritical, finite-amplitude convection. In order to test this idea and understand the phenomenon more fully a set of experiments was carried out with controlled initial conditions at a viscosity variation of 50.

The layer was left at 20 °C for 15 h and then a mask containing a single slit, 4 cm wide, across its centre was placed over the layer. The heat lamps were switched on in order to generate horizontal temperature gradients in the fluid under the illuminated slit. After one hour the water-bath temperatures were set to their final values. When convection appeared, as a single rising region under the slit in the mask, the heat lamps and mask were removed and the evolution of the pattern observed. Experiments were carried out at different Rayleigh numbers above and below the value of R_D obtained previously.

In experiments above R_D a single roll initially formed under the slit in the mask. Later further rolls formed either side of this roll and the convective pattern gradually propagated from the centre outwards (figure 9). As in the experiments from random initial conditions, the rolls broke down into hexagons until the whole layer was covered with a uniform hexagonal pattern. The wavenumbers of the original rolls and the final hexagons were also the same as in the random case. In the experiments carried out below R_D the initial roll formed as before but died away when the forcing from the heat lamps was removed.

These experiments indicate that a disturbance initiated by horizontal temperature gradients can resonate with finite-amplitude, subcritical convection and so continue to grow once the forcing is removed. Below R_D convection remains localized to the origin of the driving temperature gradients and dies away once these are removed. In the experiments with random initial conditions, convection remained as boundary rolls confined to the edges of the tank when the Rayleigh number was below R_D. At higher Rayleigh numbers these rolls resonated with the subcritical, finite-amplitude state, which existed because of the variable viscosity, and propagated into the interior of the layer.

The occurrence of these subcritical instabilities driven by temperature perturbations at the side walls are probably the reason for the confusion of Somerscales & Dougherty (1970) in defining a critical Rayleigh number. They found that, for a fluid with a weakly temperature-dependent viscosity, rolls appeared at the sidewalls and propagated towards the centre as the Rayleigh number was increased. At $R = 1670$ their rolls broke down into hexagons which persisted until the Rayleigh number was raised above a certain value when they broke down into rolls.

Stengel *et al.* (1982) carried out experiments to measure the critical Rayleigh number in a laboratory experiment using glycerine with a viscosity variation of up to 3000. They determined the onset of convection by both visual observations and changes in the heat flux and noted that 'at small to moderate c in glycerol, an initial pattern of rolls always broke up into hexagons after the apparatus had been allowed

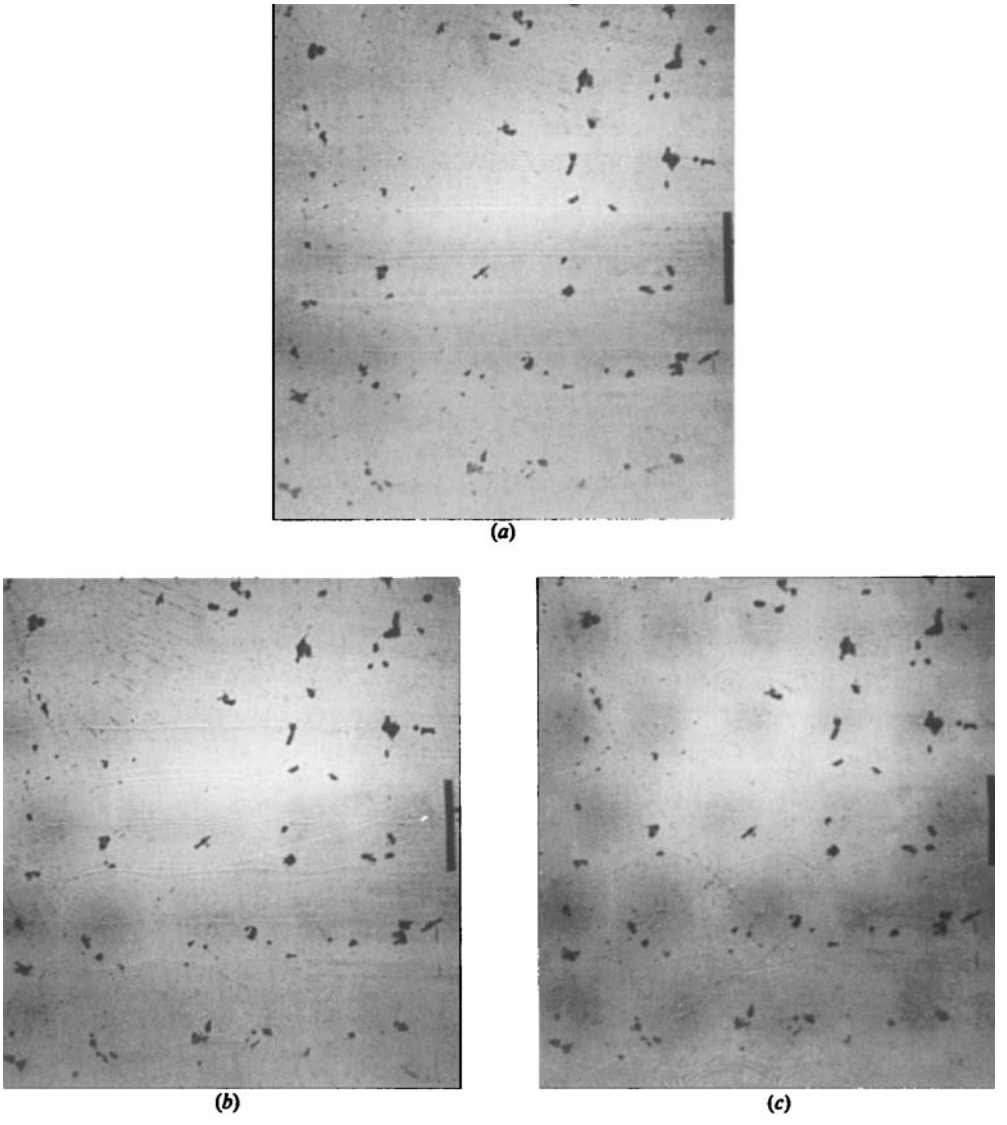

FIGURE 9. The growth of a convective roll induced by horizontal temperature gradients from a set of heat lamps and a mask. The Rayleigh number of the fluid was 1880, which is above R_D, and the viscosity variation was 50. The marker was twice the fluid depth. (*a*) After 2 h new rolls had formed either side. (*b*) After 7 h the rolls were seen to be breaking down into hexagons. (*c*) After 18 h the final hexagonal pattern.

to sit with constant ΔT for several hours'. Their parameter c was $\ln(\nu_{max}/\nu_{min})$. This behaviour could well be an example of the type of instability discussed above.

The set of experiments presented above illustrates some of the problems involved in measuring a critical Rayleigh number for a variable-viscosity fluid. Using a change in the Nusselt number to determine the onset of convection has the advantage that it is a more sensitive method than visual observation. However, the method cannot discriminate between a change in the Nusselt number due to the onset of 'normal' convection and subcritical convection excited by horizontal temperature gradients

at the boundaries. For an accurate determination of R_c great care must be taken to avoid any such horizontal temperature gradients at the edges.

The results presented here indicate that there is an increase in the critical Rayleigh number as the viscosity variation is increased up to 50. The measured values are about 14% less than the calculated ones, which is probably due to the neglect of the finite conductivity of the boundaries and the unknown temperature dependence of α and C_p in the calculations. The determination of the critical Rayleigh number is complicated by the occurrence of subcritical instabilities excited by horizontal temperature gradients at the boundaries.

4. Planforms of variable viscosity flows

At low Rayleigh numbers in a uniform-viscosity fluid the only stable convective planform is rolls within a limited bandwidth of wavenumbers (Busse 1967*a*; Busse & Whitehead 1971). The effect of a small viscosity variation is to reduce the Rayleigh number, R_B, of the bimodal transition, and the existence of a new stable planform, hexagons, at low Rayleigh numbers and large viscosity variations (Richter 1978).

The definition of stability must have a subjective element as a pattern can break down by a uniform process or though the action of dislocations triggered at the edges by the imperfect packing in the finite layer. These dislocations work their way in from the sides and rearrange a pattern that would otherwise remain unchanged. The definition of stability chosen was that the pattern should remain unchanged for at least 24 h ($d^2/\kappa \approx 7$ h). At small viscosity variations rolls and the bimodal pattern were observed with hexagons stable near R_c. However, in experiments with viscosity variations greater than 6 a new planform of squares was found to be stable. The stable planforms are illustrated below.

4.1. *Rolls*

Rolls consist of rising and sinking fluid in a two-dimensional pattern (figure 10*a*). They are the stable planform for a range of Rayleigh numbers and wavenumbers in flows with a small viscosity variation. Richter (1978) found that these variable-viscosity rolls were subject to the same instabilities as those in a constant-viscosity fluid although there was a reduction in R_B with increasing viscosity variation.

4.2. *The bidomal pattern*

This pattern consists of a set of primary rolls with a weaker, perpendicular set of larger-wavenumber secondary rolls (figure 10*b*) and represents the transition to a three-dimensional planform. In the illustrated pattern the viscosity in the cold boundary layer is an order of magnitude greater than that in the hot boundary layer, and yet an enlargement of the picture (figure 10*c*) shows the goblet-shaped streak patterns to be identical to those observed by Busse & Whitehead (1971).

4.3. *Squares*

A typical example of the new square planform (figure 10*d*) clearly illustrates a discrete rising plume at the cell centre surrounded by four sinking sheets. This structure is in contrast to the proposed square pattern for a constant-viscosity fluid (Rayleigh 1916; Chandrasekhar 1961) which consists of squares of alternately rising and sinking fluid in a chequerboard fashion. The square pattern was also found to exist as a subcritical, finite-amplitude state when it still displayed the same features of isolated rising plumes.

In constant-viscosity convection the only pattern to resemble squares is a bimodal pattern with equal primary and secondary wavenumbers. However, Whitehead & Parsons (1978) showed that a square bimodal pattern was not stable below a Rayleigh number of 130000 and the variable-viscosity squares do not show the asymmetry in convective amplitude seen in the bimodal flow. Additionally, in uniform-viscosity flows the bimodal pattern is thought to be a boundary-layer instability which develops when $R > 22600$ whereas squares were observed at, and below, R_c when the boundary layers have not formed. The reduction in R_B observed by Richter (1978) is insufficient to account for the existence of stable squares around R_c. Streak patterns in the syrup give some indication of the fluid flow but their interpretation is difficult as they can be extremely complex (figure 10*e*).

The new square planform does seem to be distinct from a bimodal pattern of equal wavelengths. In the square pattern observed above, the localization of the rising plumes was clearly observed when the Rayleigh number was suddenly raised from a low value. The rising regions became more visible as the temperature contrast increased but initially they retained their original circular shape. As the Rayleigh number was further increased the central rising jets elongated until a continuous roll could be seen at a Rayleigh number of ≈ 25000 and the pattern began to resemble a bimodal flow (White 1981). Busse & Riahi (1979) and Proctor (1981) have calculated that squares should appear in a constant-viscosity fluid with fixed flux boundary conditions. However, these squares consist of a pattern of alternative squares of rising and sinking fluids, unlike the squares above where there is a central rising region surrounded by sinking fluid. Busse & Frick (1985) predict the existence of a square pattern for viscosity variations greater than 2 in their analysis of a linear viscosity variation.

4.4. *Hexagons*

The hexagons seen here (figure 10*f*) are identical to those seen by Richter (1978). Each cell consists of a central rising plume surrounded by six sinking sheets. Distortions of the pattern occur at the edges where imperfect packing occurs. The streak patterns observed (figure 10*g*) suggest that the fluid flow is similar to that proposed by Chandrasekhar (1961). As predicted by Busse (1967*b*) hexagons were also observed as a subcritical, finite-amplitude state.

4.5. *Triangles*

In experiments with hexagons at high Rayleigh numbers a tendency to form a triangular planform was observed. To investigate this further, a regular triangular pattern was induced (figure 10*h*). The pattern consisted of rising regions centred in an hexagonal array surrounded by three sinking sheets forming an equilateral triangle. The pattern was very unstable at low Rayleigh numbers but remained for more than 10 h at a Rayleigh number of 26000 and a viscosity variation of 50. The cell structure observed is very similar to that proposed for triangles by Chandrasekhar (1961).

4.6. *Spokes*

In constant-viscosity convection the spoke pattern, or multi-modal flow, is the result of the breakdown of the bimodal pattern at a Rayleigh number of $\approx 10^5$. It consists of rising and sinking fluid arranged in a 'time-dependent' spoke-like pattern. 'Time dependent' is used here to describe the planform at a given point. The gross structure of the pattern remains the same but the features move around. Time-lapse movies have shown periods of relative stability followed by rapid change and then further stability. The same features were seen in the variable-viscosity experiments at

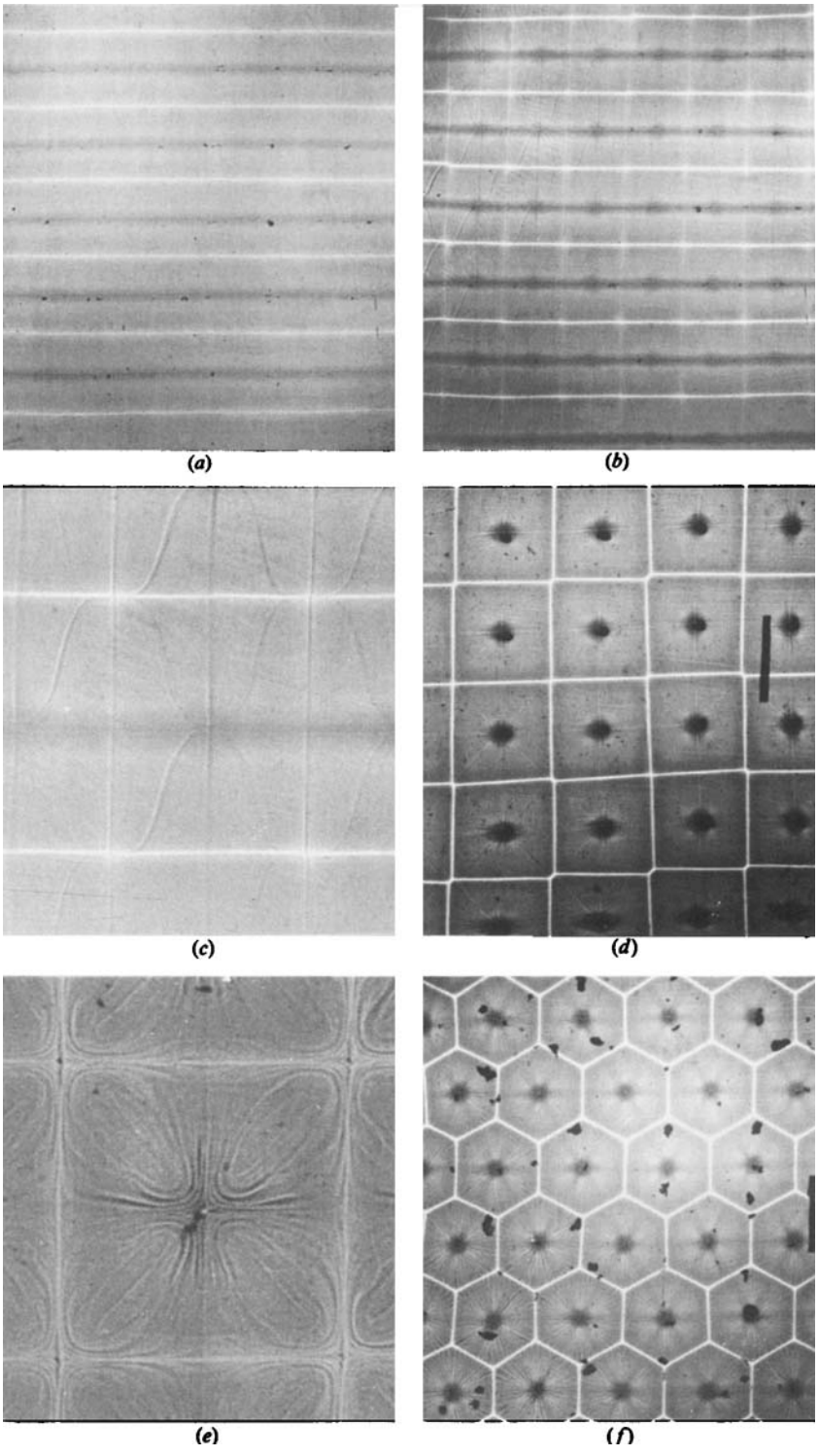

FIGURE 10*a–f*. For caption see facing page.

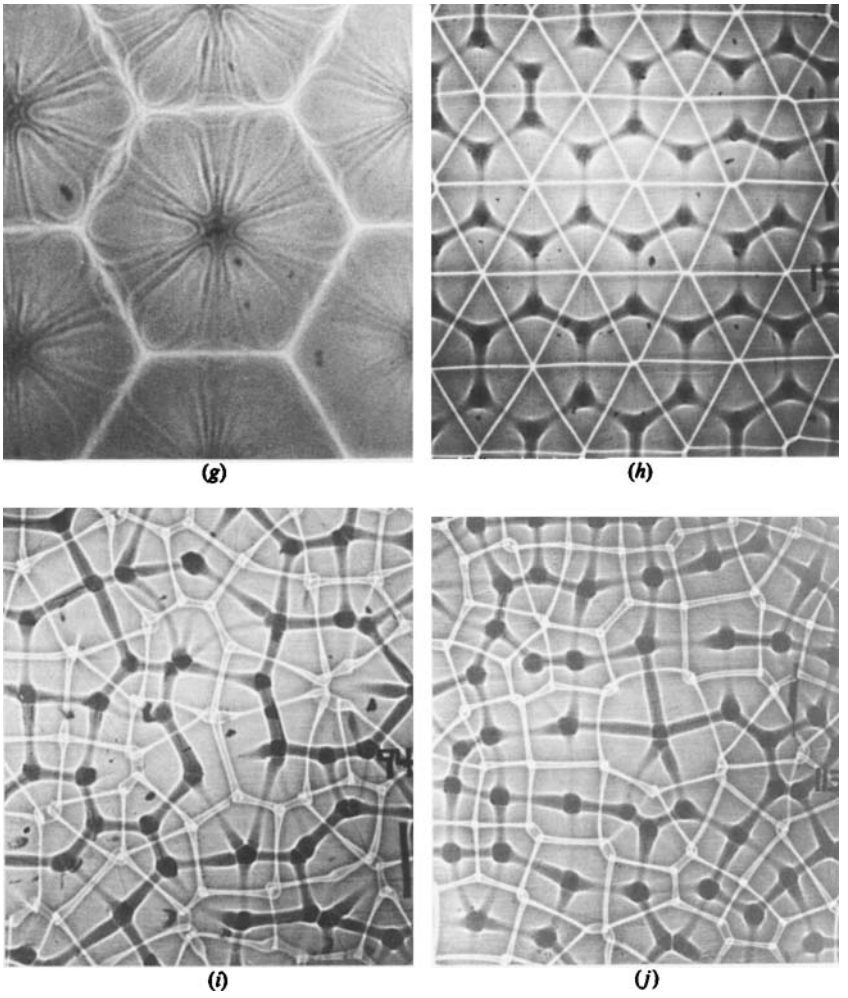

FIGURE 10. The stable planforms. (*a*) Rolls with $R = 9700$, $k = 3.14$ and a viscosity variation of 4.5 seen after 8 h. (*b*) The bimodal pattern, formed from rolls with $k = 3.14$, at $R = 11000$ and with a viscosity variation of 10 seen after 23 h. (*c*) An enlargement of (*b*) to show the 'goblet'-shaped streak pattern. (*d*) A square planform, with $R = 15600$, $k = 2.86$ and a viscosity variation of 50 seen after 24 h. (*e*) Streak patterns in squares with $R = 5800$, $k = 3.14$ and a viscosity variation of 50. (*f*) Hexagons with $R = 9300$, $k = 3.62$ and a viscosity variation of 50 seen after 4 h. (*g*) Streak patterns in hexagons with $R = 13400$, $k = 3.62$ at a viscosity variation of 10. (*h*) Triangles with $R = 25800$, $k = 3.0$ and a viscosity variation of 50 seen here after 10 h. (*i*) A spoke pattern at $R = 63300$ with a viscosity variation of 51 after 17 h. (*j*) A spoke pattern with $R = 30600$ and a viscosity variation of 1020 after 28 h, All the experiments were in a 5 cm layer, except for (*i*) and (*j*) which were in a 6 cm layer; the marker, where shown, was 10 cm.

Rayleigh numbers as low as 30000 and resulted from the breakdown of the previously described patterns (figure 10*i*, *j*). The most remarkable feature of these pictures is their similarity to the constant-viscosity flows, despite a viscosity variation of up to three orders of magnitude. The only easily discernible difference from the constant-viscosity flow is a small reduction in the horizontal scale with increasing viscosity variation. Thus at low Rayleigh numbers a variable viscosity produces new planforms but, even for large variations in viscosity, once the Rayleigh number exceeds ≈ 30000 the familiar spoke pattern develops.

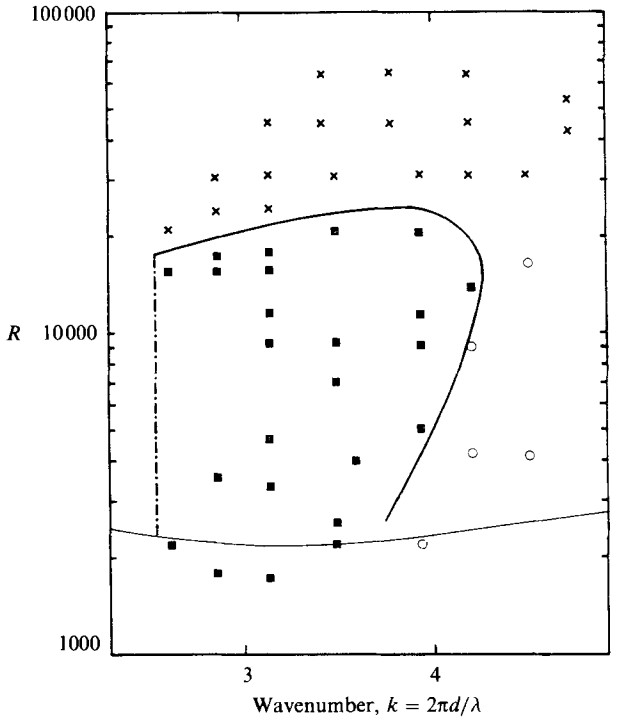

FIGURE 11. The experimentally determined stability region of the square convection pattern at a viscosity variation of 50 ± 3: ■, stable squares; ○, breakdown by cell fusion; ×, breakdown by various local processes. The dot–dashed line is the limit, set by the mosaic instability, of the smallest-wavenumber squares that can be induced, and the lower curve represents the neutral curve for a syrup-type viscosity with a variation of 50.

5. The stability of squares

In the following experiments a regular convection pattern was induced using the techniques described in §2. The forcing was removed and the planform was allowed to evolve with time in order to study its stability. The experiments were conducted at a fixed viscosity variation of either 50 or 1000, whilst the Rayleigh number and wavenumber were varied between runs. The latter set of experiments used a 6 cm deep layer.

The stability of squares as a function of R and k, where $k = 2\pi d/\lambda$ and λ is the separation of adjacent rising regions, is shown in figures 11 and 12. The limits of the stable region are set by the occurrence of several different instabilities, described below. The neutral curve included in these figures is from linear stability calculations for a fluid with a syrup-type viscosity variation (White 1981). Inside the stable region squares were observed to remain unchanged for up to a week.

The most striking difference between these observations and those for constant-viscosity rolls is the occurrence of subcritical convection, predicted by Busse (1967*b*), but in the form of hexagons, not squares. The subcritical squares observed were induced above R_c and then the Rayleigh number was reduced. Even at the lowest Rayleigh numbers for which these squares were observed, they remained perfect and did not adjust to hexagons. The other most noticeable feature of figures 11 and 12 is the shift in the range of stable wavenumbers to larger values and that they are no longer centred about k_c as in the case of constant-viscosity rolls. The stable

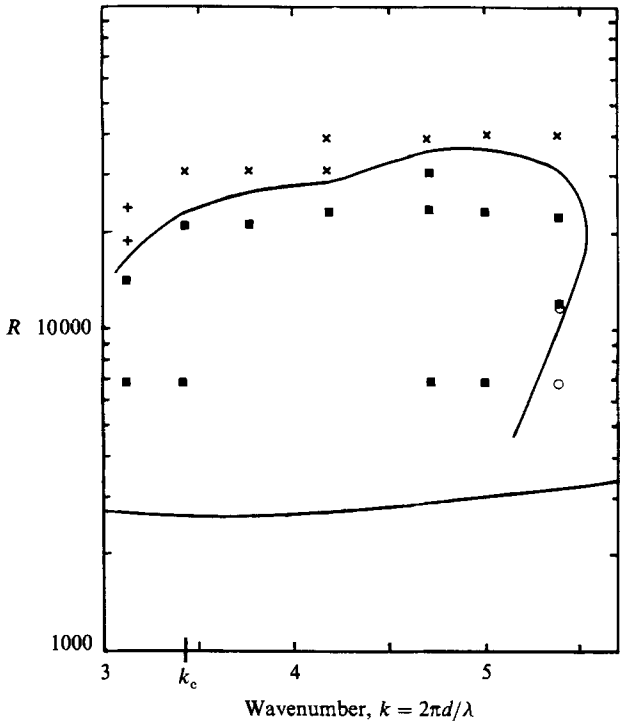

FIGURE 12. The stability region for squares in flows with a viscosity variation of 1000 ± 50; ■, stable squares; ○, cell fusion; ×, breakdown by various local processes; + symmetric cell splitting. The neutral curve (the lower curve) and k_c are for a syrup-type viscosity with a variation of 1000.

bandwidth at a viscosity variation of 1000 shows a more marked shift to larger wavenumbers than those with a viscosity variation of 50. At a viscosity variation of 1000 squares with k as large as 5.4 were found to be stable and those with even higher wavenumbers may also be stable but it was not possible to induce them since the thermal inertia of the system was such that the water-bath temperatures could not be brought to their final values before convection started at a lower viscosity variation than planned. Consequently the squares broke down before they reached the final state at which they may have been stable.

The transitions responsible for the boundaries of the stable region were essentially the same in both cases, which is surprising considering the twenty-fold increase in the viscosity variation between the two sets of experiments. The result of all transitions caused by moving out of the top of the stable region was to produce a time-dependent spoke pattern with a gradual change in the exact nature of the breakdown between small and large k. One interesting feature observed was the role of symmetry in the break down of small-wavenumber, large-viscosity-variation squares just above the stable region. It is also interesting to note that the transition from a regular square pattern to a more disordered and time-dependent flow occurs at $R \approx 25000$, which is very similar to the Rayleigh number at which the bimodal instability occurs in constant-viscosity rolls. Richter *et al.* (1983) report a change in the Rayleigh number–Nusselt number relationship in variable-viscosity convection at a Rayleigh number of 20000–30000, indicating that the change in planform is associated with a change in the thermal structure. The spoke pattern would appear to be less efficient at transporting heat than a square pattern at the same Rayleigh number. At low

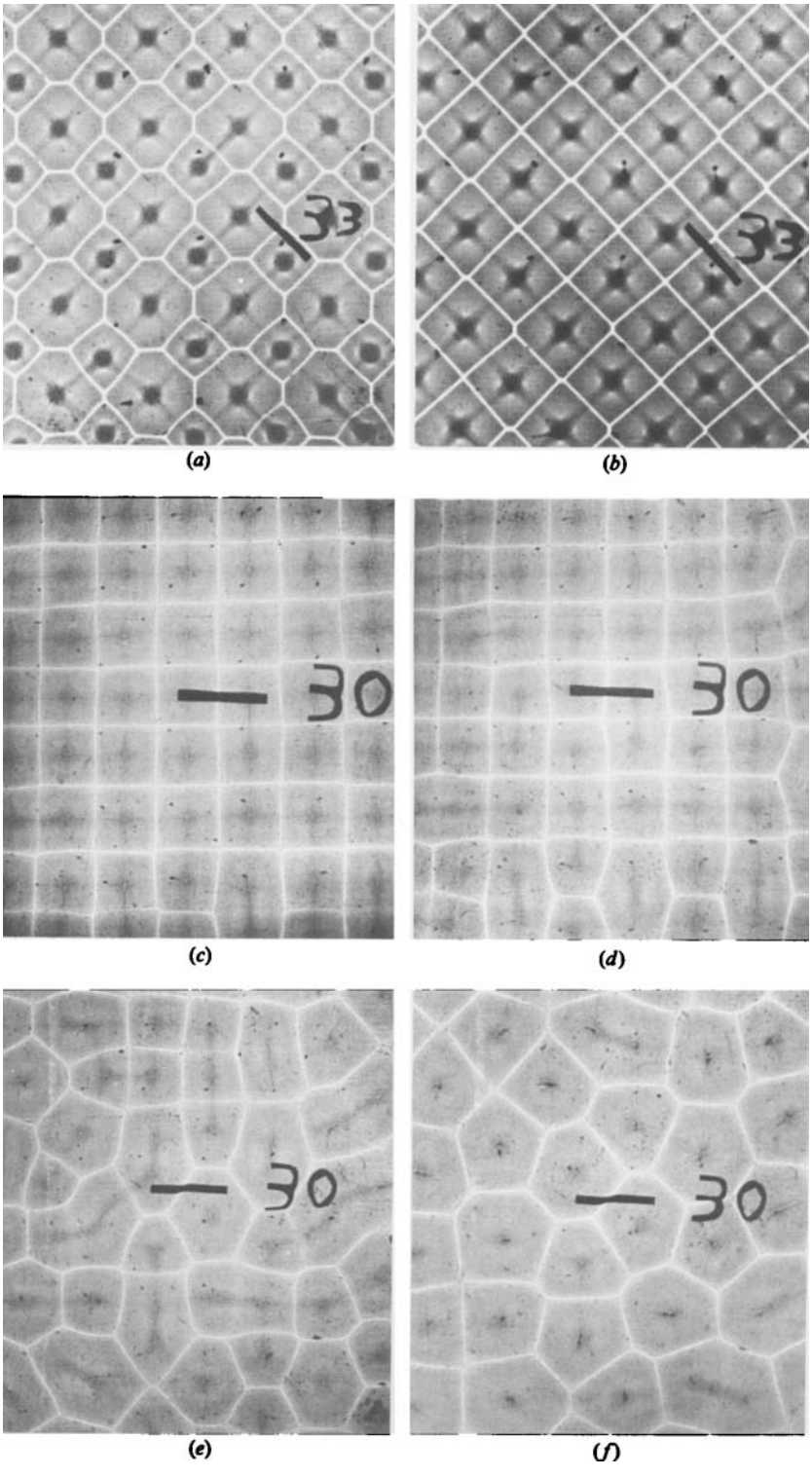

FIGURE 13*a–f*. For caption see facing page.

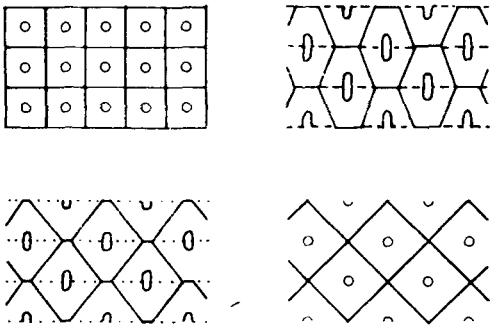

(*g*)

FIGURE 13(*a*, *b*). The mosaic instability observed in squares with $k = 2.62$ induced at a Rayleigh number of 14800 and a viscosity variation of 50. (*a*) The initial appearance of the pattern with rising regions developing at the corners of the induced squares. (*b*) After 4.2 h the small squares have grown at the expense of the octagons to produce a final square pattern with a wavenumber increased by $\sqrt{2}$. (*c–g*) Cell fusion seen in squares with $R = 4150$ and $k = 4.49$ at a viscosity variation of 50. (*c*) The initial square pattern showing slight distortions after 1.2 h. (*d*) A regular breakdown is seen along the bottom after 3 h. (*e*) A random breakdown over the rest of the layer produced an irregular pattern after 7.8 h. (*f*) A final pattern of irregular polygons after 22.7 h with a wavenumber decreased by about $\sqrt{2}$. (*g*) Schematic diagram to illustrate how regular cell fusion could produce a final pattern of squares with a wavenumber reduced by a factor of $\sqrt{2}$ orientation at 45° to the original pattern. The marker is twice the fluid depth.

Rayleigh numbers the transitions act upon a square pattern outside the stable area to produce a new set of squares or polygons with a wavenumber inside the stable region. This behaviour is very similar to the action of the zigzag and cross-roll instabilities in low-Rayleigh-number-constant-viscosity convection.

5.1. *The mosaic instability*

The mosaic instability sets the small-wavenumber limit of stable squares and occurred as convection first appeared. When small-wavenumber squares were initiated at a high Rayleigh number (ΔT was changed from being subcritical to a final value corresponding to a high Rayleigh number) and hence a high growth rate, convection was observed to start as rising jets at points on a square array defined by the mask (figure 13*a*, *b*). As the diagonal separation between these rising regions was large compared with the layer depth, other rising regions formed on these diagonals to produce a pattern of octagons, centred on the induced rising jets, with small squares at their corners. These squares grew to produce a pattern at 45° to, and with a wavenumber $\sqrt{2}$ times, that of the original and thus moved it well into the stable region.

If a small-wavenumber square pattern was induced at a low Rayleigh number, and hence a small growth rate, the rising jets on the diagonals did not grow and desired square pattern was produced after several hours. Once the squares were established the Rayleigh number could be raised without the occurrence of the mosaic instability. Thus the mosaic instability can only occur at the start of convection when the sense of fluid motion at the corners of the induced squares is unspecified . With decreasing wavenumber the Rayleigh number below which squares must be induced to avoid the mosaic instability also decreases until, at $k \approx 2.62$, squares can only be forced at just above R_c, which sets the limit to the smallest wavenumber squares whose stability can be investigated. Any squares with $k < 2.62$ was subject to the mosaic instability at whatever Rayleigh number it was induced.

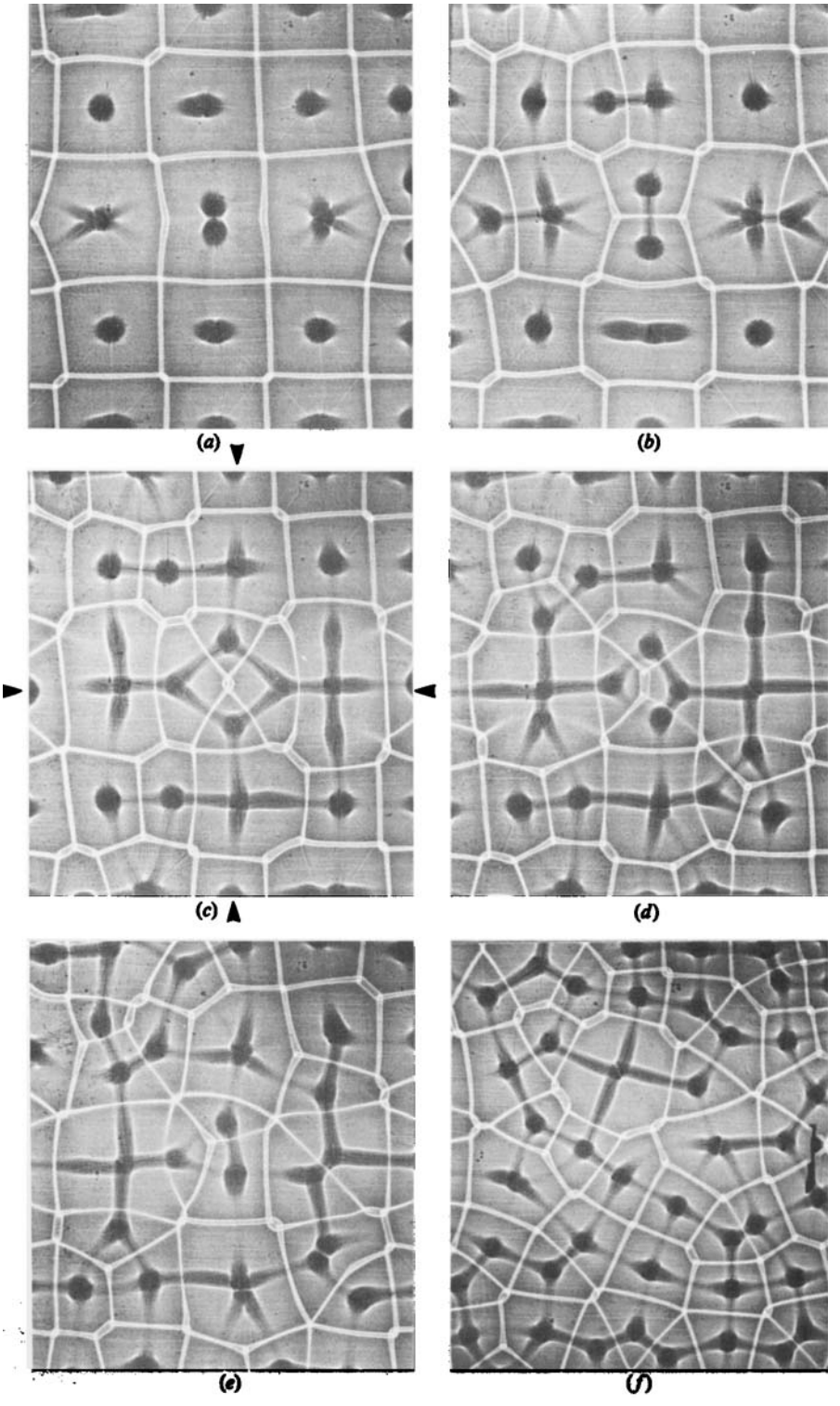

FIGURE 14*a–f*. For caption see facing page.

5.2. *Cell fusion*

Cell fusion produced a reduction in the wavenumber of the convection pattern. A sinking sheet, which made up the cell wall between two adjacent squares, began to decay and allowed the rising jets at the centres of the two cells to move together and merge, thus forming a large cell (figure 13*c–f*). The formation of a perfect square pattern, with a wavenumber smaller by a factor of $\sqrt{2}$, is possible by this mechanism (figure 13*g*) but would require large-scale regularity and uniform orientation of the breakdown of the cells. However, there was no preferred direction in the layer and whilst a regular breakdown could be seen along the bottom of the screen, it also occurred at 90° to this orientation in other parts of the layer, which resulted in a pattern of irregular polygons rather than squares. The size adjustment was as predicted for the regular breakdown and the average separation of rising regions gave $k \approx 3.1$ compared with a predicted value of $k = 3.17$.

5.3. *The transition to spokes*

The transition to spokes at high Rayleigh numbers, greater than 25000, revealed no regular transitions and the exact nature of the instabilities depended upon the wavenumber and Rayleigh number of the original squares. Full details of these instabilities can be found in White (1981).

5.4. *Symmetric cell splitting*

Symmetric cell splitting is well illustrated in a run at a viscosity variation of 1000 with $R = 23200$ and $k = 3.15$ by a series of time-lapse photographs (figure 14). The remarkable feature of this experiment was the symmetry displayed in the breakdown of the pattern, as illustrated in figure 14(*c*) where two lines of symmetry are indicated. It is difficult to understand how this symmetry can occur as it requires coordination of the pattern over long distances. Typical fluid velocities under these conditions have been estimated as 20 cm/hr and yet changes were seen to occur simultaneously and symmetrically over distances greater than 50 cm. The long-range ordering of the breakdown must be effected by forces transmitted instantaneously by the pressure field. In addition, the geometry of the rising and sinking regions perhaps set up horizontal temperature gradients that drove a large-scale flow which also helped organize the breakdown. The final pattern was a disorganized spoke flow with generally larger-wavenumber cells.

6. The stability of hexagons

The stability map for hexagons at a viscosity variation of 50 (figure 15) shows the same shift towards large wavenumbers that is evident for squares but has a slightly smaller bandwidth of stable wavenumbers. Again the stable region was bounded by the occurrence of several transitions with the existence of finite-amplitude, subcritical convection below the calculated neutral curve. Inside the stable region hexagons

FIGURE 14. Symmetric cell splitting in squares with $k = 3.15$ and $R = 23200$ and a viscosity variation of 1020. (*a*) Squares along the middle of the screen began to split after 10 h. (*b*) Squares either side of the central row were also observed to start splitting after 13 h. (*c*) The breakdown continued with remarkable symmetry. In this picture, after 15.5 h, two lines of symmetry are drawn. (*d*) After 18 h the symmetry of the pattern began to break down. (*e*) This breakdown continued and after 20.5 h the pattern was more irregular. (*f*) Finally a spoke-like flow developed after 28 h. The layer was 6 cm deep, with a 10 cm marker.

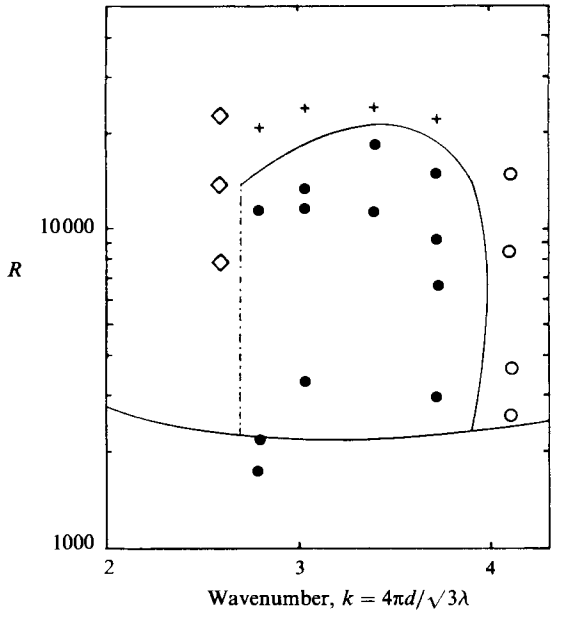

FIGURE 15. The experimentally determined stability region for hexagons at a viscosity variation of 50 ± 3: ●, stable hexagons; ◇, the mosaic instability; ○, breakdown by cell fusion; +, cell splitting. The dot–dashed line is the limit, set by the mosaic instability, of the smallest wavenumbers that could be induced.

remained unchanged for many timescales though there was a slight adjustment from the edges where the hexagonal pattern could not pack perfectly into a finite rectangular layer. Above a Rayleigh number of ≈ 20000 hexagons broke down into a more disordered time-dependent flow. There are problems in determining the stability of hexagons as it is also function of the perfection of the initial pattern due the action of dislocations initiated at the sidewalls. The breakdown of cells in the centre of the layer was the best indication of stability as they were farthest removed from the edge effects.

The three main transitions, similar to those for squares, were:

6.1. *The mosaic instability*

The mosaic instability again sets the limit to the smallest-wavenumber hexagons that can be induced. When the initial wavenumber was just outside the stable area extra rising regions formed at each vertex of the original hexagons, in a similar manner to the mosaic instability in squares. This instability leads to a hexagonal pattern with a wavenumber $\sqrt{3}$ times the original and is illustrated in figure 16. In this case the wavenumber of the resulting hexagons was outside the stable region so the hexagons broke down. Had symmetry been followed, triangles would have formed.

6.2. *Cell fusion*

Cell fusion produces a pattern of smaller-wavenumber polygons (figure 17*a*, *b*). In squares two cells condense to form a larger one with a wavenumber increased by a factor of $\sqrt{2}$. For hexagons to retain the same symmetry three cells must merge in the production of a hexagon with a wavenumber increased by $\sqrt{3}$ (figure 17*c*). Groups of three cell walls in a regular hexagonal array must break down simultaneously for the transformation to produce a regular pattern. The breakdown

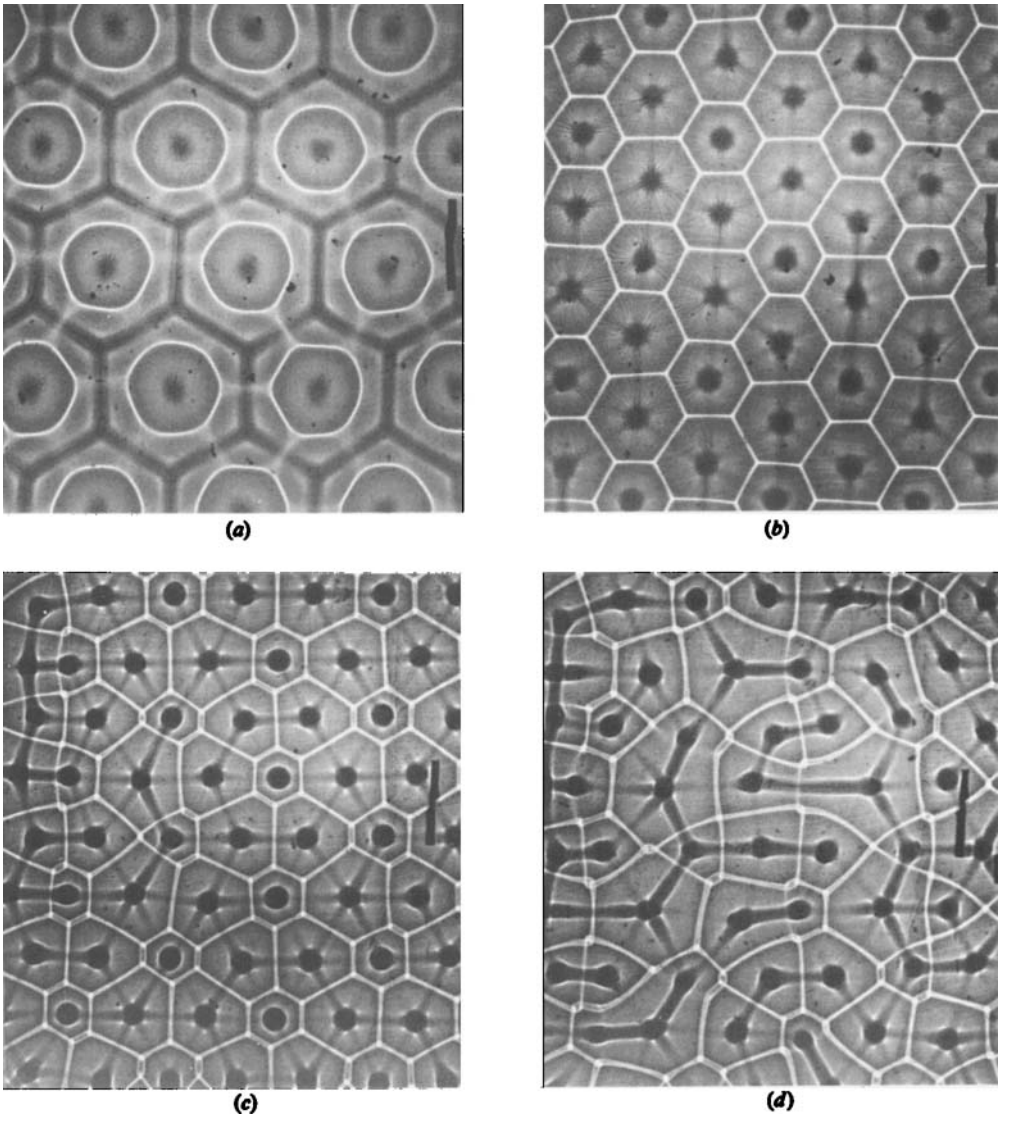

FIGURE 16 (*a*, *b*). The development of the mosaic instability in an initial hexagon pattern with $k = 2.59$ induced at a Rayleigh number of 16000. (*a*) The initial appearance of convection. (*b*) After 1.5 h a nearly regular hexagonal pattern evolved. (*c*, *d*) The further development of the mosaic instability in hexagons with an initial wavenumber of 2.59 at a higher Rayleigh number of 30 500. The original rising regions induced through the mask are those at the centres of the small hexagons. (*c*) After 2 h the initial hexagons had become smaller. (*d*) A random pattern was seen to be developed 30 min later as cell fusion continued.

of cells in the layer is not this organized and no indication of the illustrated transformation was observed.

6.3. *Cell splitting*

Cell splitting was very similar to that seen in squares (figure 18). This breakdown initially produced a disordered pattern of larger-wavenumber polygons, including many squares, with the eventual development of some spoke-like features consisting of a ring of nearly triangular cells.

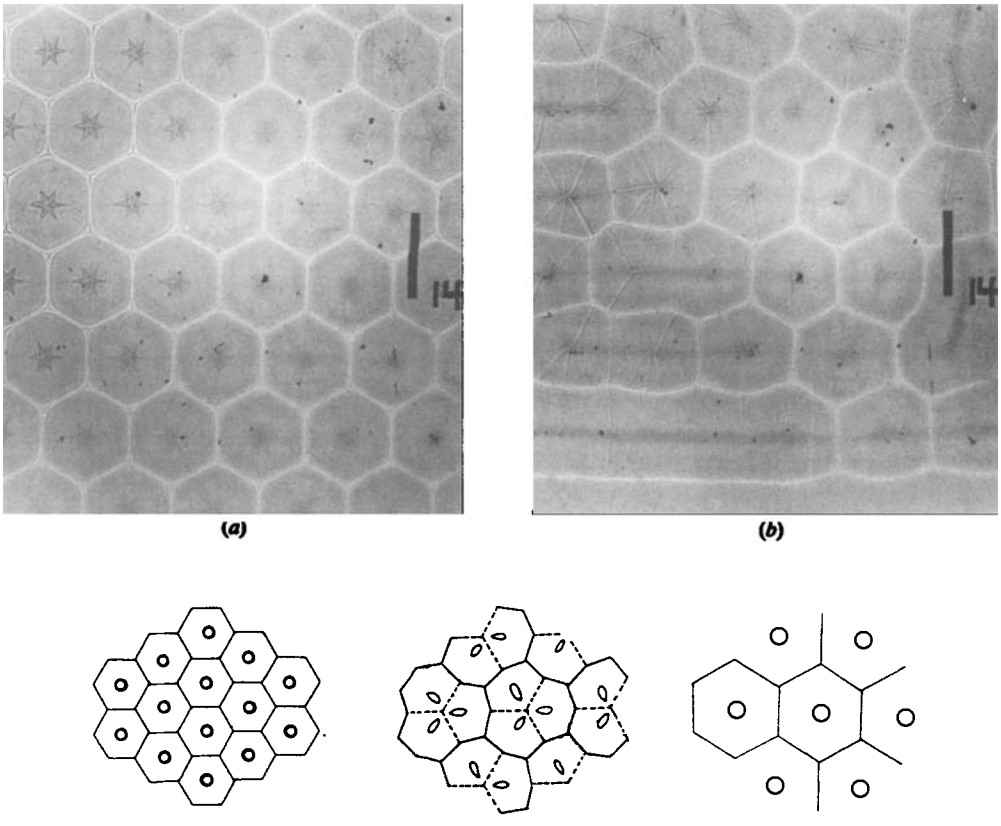

FIGURE 17. Cell fusion in hexagons with $k = 4.54$, $R = 4600$ and a viscosity variation of 50. (*a*) The initial pattern after 30 min. (*b*) A set of irregular polygons after 17 h. (*c*) An illustration of the breakdown by cell fusion required to produce hexagons with a wavenumber reduced by $\sqrt{3}$.

7. Vertical temperature profiles

The reduction in the horizontal scale of the fluid motions as the viscosity variation is increased should be associated with a change in the thermal structure of the cell. In order to study these changes vertical temperature profiles were obtained for square cells at different viscosity variations using a small probe consisting of a thermistor, calibrated to 0.01 °C, mounted at the end of a 35 cm length of 1.5 mm diameter tube which could be swung into position in the layer and locked. A very low-speed motor then wound in a thread which raised the probe through the layer. Profiles were taken at a Rayleigh number of around 20000, for a viscosity variation of ≈ 25, ≈ 150, and ≈ 1000. Figure 19 shows the vertical temperature profile obtained at a point between the sinking and rising regions of a square at a Rayleigh number of 23700 and a viscosity variation of 1070. The existence of a cold, stagnant, upper boundary layer is immediately obvious. The intercepts on the temperature axis at $d = 0$ and $d = 6$ cm agree with the calculated boundary temperatures, showing that Wray's (1978) Nusselt-number relationship is accurate in flows with a viscosity variation as large as 1000. Below the cold boundary layer the profile is stably stratified and nearly isothermal with the hot boundary layer at the base of the layer.

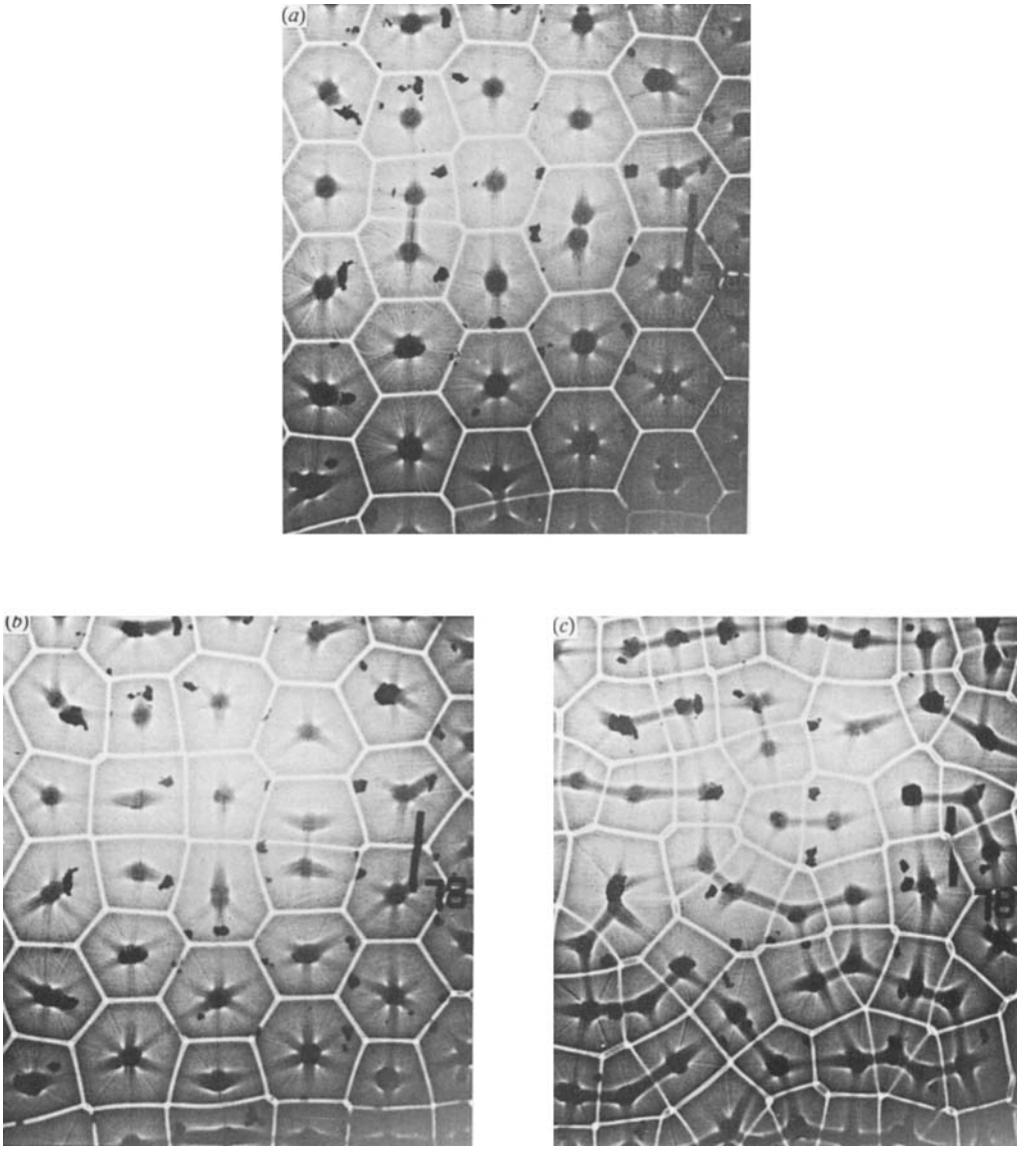

FIGURE 18. Cell splitting observed in hexagons with $k = 3.03$, $R = 24200$ and a viscosity variation of 50. (*a*) After 2 h the rising regions at the centres of some hexagons had split in two. (*b*) After 4 h further splitting had taken place. (*c*) The final pattern of irregular polygons and some spoke-like features was time-dependent and is seen here after 22 h.

The temperature profiles were then non-dimensionalized using the layer depth and the calculated temperature difference. The vertical temperature profiles through cold, intermediate and hot regions are shown in figure 20 for squares with $R = 24000$ and $\nu_{\max}/\nu_{\min} = 130$. To allow better comparison between experiments at different viscosity variations an average of the curves through the three regions was taken and plotted for each of the three viscosity variations considered (figure 21). These are not true horizontally averaged vertical temperature profiles as they were not weighted by the amount of fluid at each of the different temperatures.

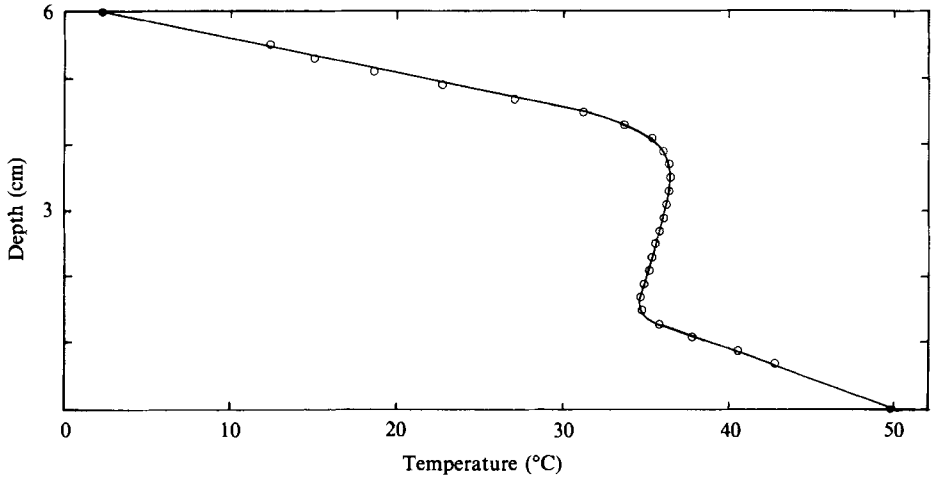

FIGURE 19. An experimentally determined temperature profile through a region between rising and sinking plumes in a square with $R = 23700$ at a viscosity variation of 1070. The open circles are the experimental results, the two closed circles are the calculated boundary temperatures. The development of a thick, stagnant cold boundary layer is immediately obvious.

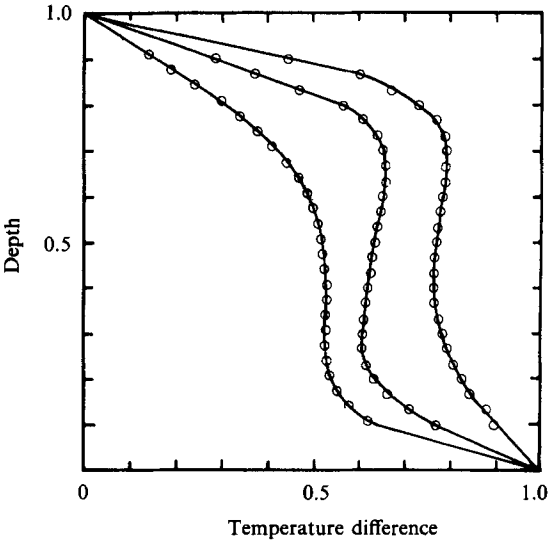

FIGURE 20. Non-dimensionalized vertical temperature profiles through hot, intermediate and cold regions of a square cell with $R = 24000$ and a viscosity variation of 130.

As expected the cold boundary layer is seen to thicken as the viscosity variation increases. In addition the temperature of the nearly isothermal central region, θ_1, also increases with increasing viscosity variation. In flows with larger viscosity variation the convective motions become confined to the hotter, less viscous part of the cell. This confinement produces the observed reduction in the horizontal wavelength of the convective planform. The results reported by Richter *et al.* (1983), who used the resistance of a fine platinum wire to measure the horizontally averaged temperature of convective flows in Golden Syrup at many different Rayleigh numbers and viscosity variations, are in good agreement with the results presented above.

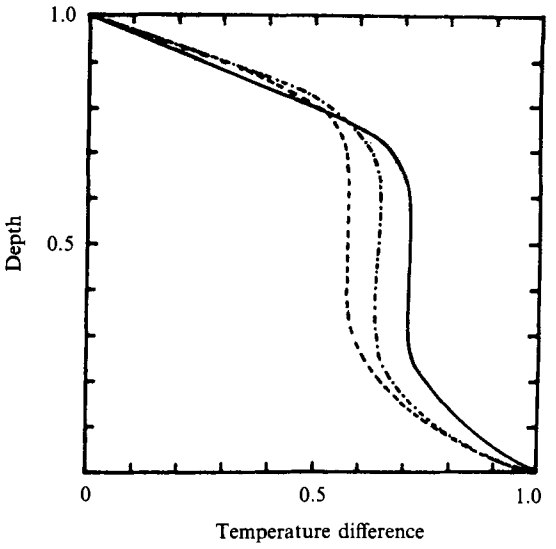

FIGURE 21. Non-dimensionalized averages of the vertical temperature profiles through hot, cold and intermediate regions for experiments with three different viscosity variations: ——, $R = 23700$, viscosity variation 1070; — · — · —, $R = 24000$, viscosity variation 130; – – – –, $R = 20400$, viscosity variation 25. The internal temperature increases with increasing viscosity variation.

Convection with a large viscosity variation produces a thick, stagnant, cold boundary layer which acts as an insulating lid to produce and increase in θ_i. A large proportion of the temperature drop across the entire layer, and thus a large proportion of the viscosity variation, occurs across this stagnant lid. The flow is restricted to the hotter, less viscous part of the cell which the horizontally averaged vertical temperature profiles show to be nearly isothermal and thus isoviscous. The confinement of the flow to the lower part of the cell is reflected in the reduction of the horizontal scale of the convective motions observed in large-viscosity-variation experiments. The similarity between a constant-viscosity spoke flow and those observed in the variable-viscosity experiments is not surprising as the temperature profiles showed a large proportion of the convecting fluid to be isoviscous.

The definition of a Rayleigh number based on the fluid properties at the mean of the boundary temperatures produces a Nusselt number–Rayleigh number relationship very similar to that for a constant-viscosity fluid (Booker 1976; Wray 1978; Richter *et al.* 1983). However, this definition does not reproduce the Rayleigh number observed for the transition between an ordered flow and the time-dependent spoke flow in a constant-viscosity fluid. The temperature profiles above clearly show that the majority of the convecting fluid is at a considerably higher temperature than the mean of the boundary temperatures. However, a Rayleigh number based on the viscosity at θ_i does not reproduce the constant-viscosity value for the transition to the spoke pattern.

8. Planform transitions with changing viscosity variation

Low-Rayleigh-number flows with a viscosity variation of 50 exhibit a different cell structure from the rolls seen at constant viscosity, with squares and hexagons as two possible stable planforms. An increase in the viscosity variation to 1000 produced no

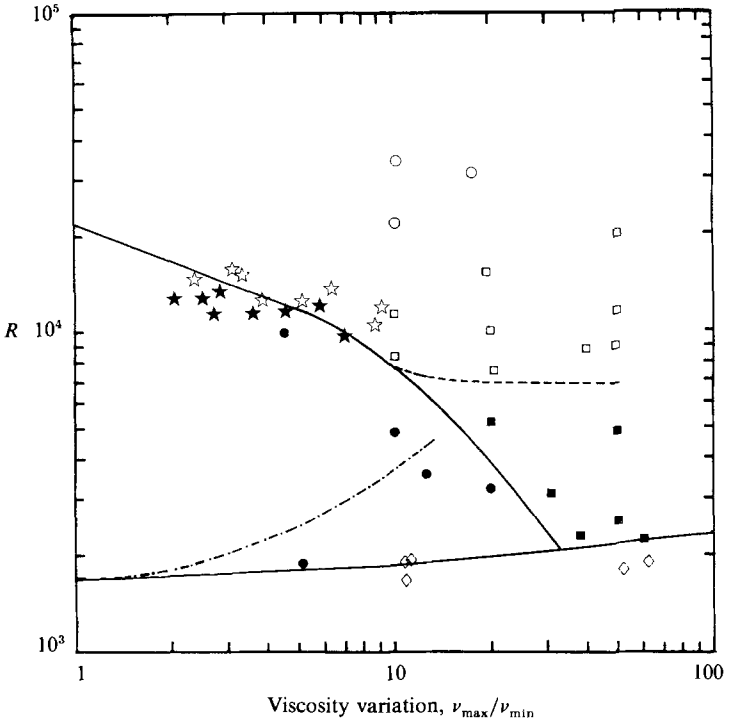

FIGURE 22. The stability map for rolls, with $k = 3.15$, as a function of the Rayleigh number and the viscosity variation: ●, stable rolls; ○, rolls that became bimodal; ◇, rolls that broke down into hexagons; ■, rolls that broke down to squares; □, rolls that became bimodal and subsequently transformed into squares. The solid and open stars represent rolls and bimodal patterns respectively from Richter's (1978) corrected data. The lower curve is the neutral curve for a syrup-type viscosity variation and the dashed line represents the Rayleigh number, R_B, of the transition of rolls to a bimodal pattern at high viscosity variations. The dot–dashed line represents the theoretical Rayleigh number at which rolls break down to hexagons (Palm *et al.* 1967).

new stable planforms although there is a further reduction in the horizontal scale of the fluid motions. In order to investigate the transitions between constant- and variable-viscosity planforms a regular convection pattern with a fixed wavenumber of 3.14 was induced using the techniques described in §2 and sets of experiments were carried out to determine the stability of rolls, squares, and hexagons as a function of the viscosity variation and Rayleigh number. Full details and examples of all the transitions can be found in White (1981) and only the most significant are included here.

8.1. *The stability of rolls*

The experiments to determine the stability of rolls confirmed Richter's (1978) work and showed that R_B decreased with increasing viscosity variation (figure 22). In addition the stable region was bounded by a transition to hexagons at a low Rayleigh numbers and to a new planform of squares at large viscosity variations.

8.1.1. *The bimodal instability*

This appeared identical to that observed in a constant-viscosity fluid. At Rayleigh numbers just above R_B the cross-roll component gradually appeared over several hours and the characteristic 'goblet' streak pattern was clearly visible. The transition was completely reversible as the cross-roll component died away when the

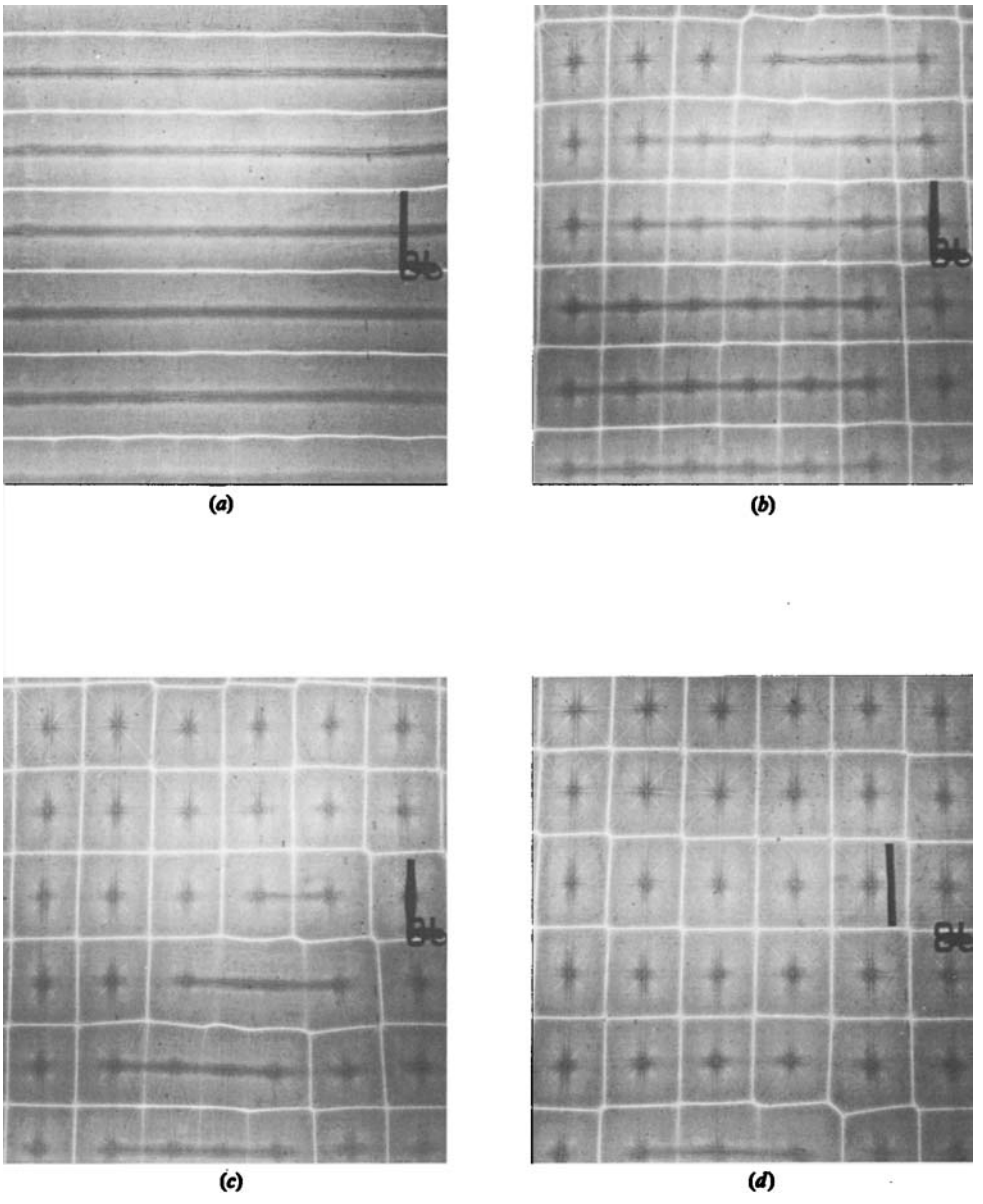

FIGURE 23. The bimodal instability in rolls with $R = 9900$ and a viscosity variation of 20.2. (*a*) After 4 h the rolls became slightly distorted. (*b*) After 27 h a bimodal pattern had formed with a dislocation in the cross-rolls. (*c*) After 50 h the dislocation had propagated in favour of smaller-wavenumber cross-rolls and an almost square pattern formed behind it. (*d*) Finally, a regular pattern of nearly square cells developed after 101 h.

Rayleigh number was reduced below R_B. The value of R_B was observed to fall with increasing viscosity variation until $\nu_{max}/\nu_{min} = 10$ when $R_B \approx 8000$. There was little further reduction in R_B as the viscosity variation was increased beyond this value and when $\nu_{max}/\nu_{min} = 20$ the bimodal transition occurred at a Rayleigh number of about 7500. The experiments show a good agreement with Richter's (1978) data, which has been corrected to take into account the temperature drop across the glass boundaries of his apparatus (White 1981).

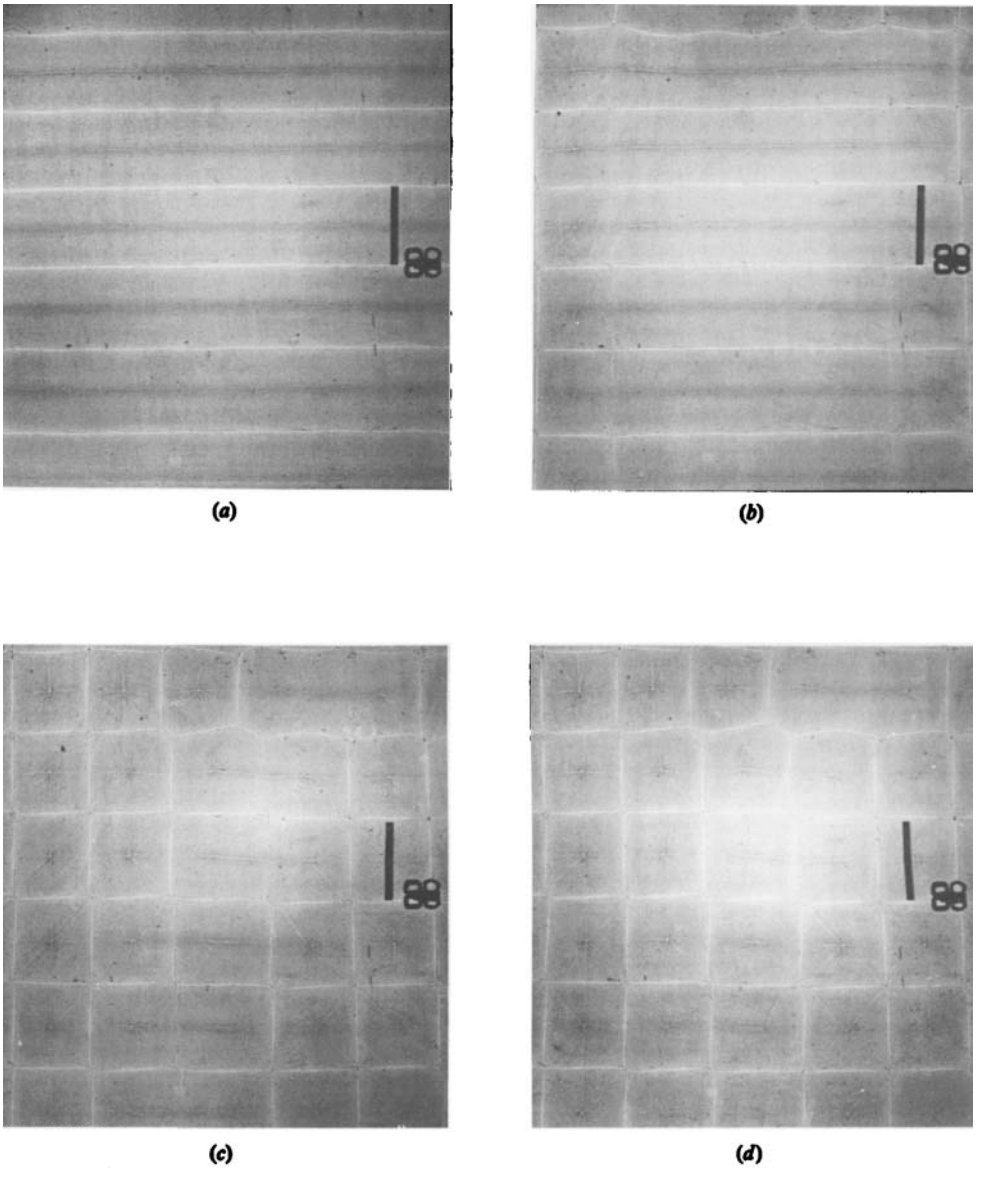

FIGURE 24. The breakdown of rolls to squares at a viscosity variation of 20 and $R = 3330$. (*a*) The initial rolls after 2 h. (*b*) Squares were observed to form at the edges after 26 h. (*c*) The squares propagated into the interior of the layer and after 67.5 h nearly all the layer was covered. (*d*) The experiment was terminated after 74 h.

The bimodal pattern formed from rolls at a viscosity variation greater than 10 and Rayleigh numbers less than 20000 was itself unstable. Dislocations in the cross-rolls propagated in favour of smaller wavenumbers until the pattern had adjusted itself such that the cross-roll component had a wavenumber nearly equal to that of the original rolls and an almost square pattern resulted. In addition to the adjustment in the cross-rolls, the primary rolls were observed to break-up into discrete rising jets at the centres of the square cells (figure 23). At Rayleigh numbers above 20000 this transition to squares was not observed.

Richter (1978) argued that the reduction in R_B was due to the reduced viscosity of the hot boundary layer, as by redefining the Rayleigh number using an estimated mean viscosity for the hot boundary layer he found that the values of R_B were close to the constant-viscosity value of 22600. However, the results above show a greater reduction in R_B with increasing viscosity variation and consequently Richter's modified Rayleigh number no longer produces a value of R_B close to that for a constant-viscosity fluid. The averaged vertical temperature profiles for variable viscosity convection showed an increase in θ_i above the constant-viscosity value of 0.5. If the viscosity at θ_i is used in defining the Rayleigh number a higher value is produced for R_B but again the value is much lower than R_B for a constant-viscosity fluid.

8.1.2. *The square instability*

This occurred in flows with $R < R_B$ and a viscosity variation greater than 10. A set of squares formed down the edges of the tank and propagated inwards (figure 24). Their rate of propagation was a function of both the Rayleigh number and viscosity variation. The larger the Rayleigh number and higher the viscosity variation the quicker the squares formed, indicating that the squares are not forced by the lateral boundaries but that the edge effects of the finite layer allow the initiation of an adjustment to an unstable pattern. A perfect pattern of rolls in a larger tank may have remained stable to slightly larger viscosity variations than were observed.

8.2. *The stability of squares*

The existence of the new, stable, square pattern is a consequence of the temperature-dependent viscosity of the fluid. At sufficiently high viscosity variations (> 200) a regular square pattern formed from random initial conditions. In this study of the stability of squares as a function of the Rayleigh number and viscosity variation, the stable region (figure 25) was bounded from below by the presence of subcritical, finite-amplitude disturbances and above by the occurrence of instabilities which led to three other planforms.

8.2.1. *The transition to spokes*

This occurred by the mechanisms described by White (1981) and the Rayleigh number of the transition is seen to drop with increasing viscosity variation (figure 25). This drop is not due to a reduction in the stability of squares but is a result of the shift of the stable band of wavenumbers to larger values with increasing viscosity variation. In this study only one wavenumber, $k = 3.14$, was used, which is not the most stable at high viscosity variations.

8.2.2. *The transition to a bimodal pattern*

This occurred when the rising jets at the centre of a line squares joined up to form a dominant roll (figure 26). The cell walls at 90° to this main roll simultaneously died away to be replaced by cells with a larger wavenumber.

8.2.3. *The transition to rolls*

This was seen when the rising regions at the centres of a line of cells joined together to form a continuous roll and convective motion at 90° to these rolls died away completely. An experiment with $R = 5850$ and $\nu_{max}/\nu_{min} = 10$ was right at the edge of the stability boundary (figure 27) and after 48 hours only half of the square pattern remained as the rest had transformed into rolls.

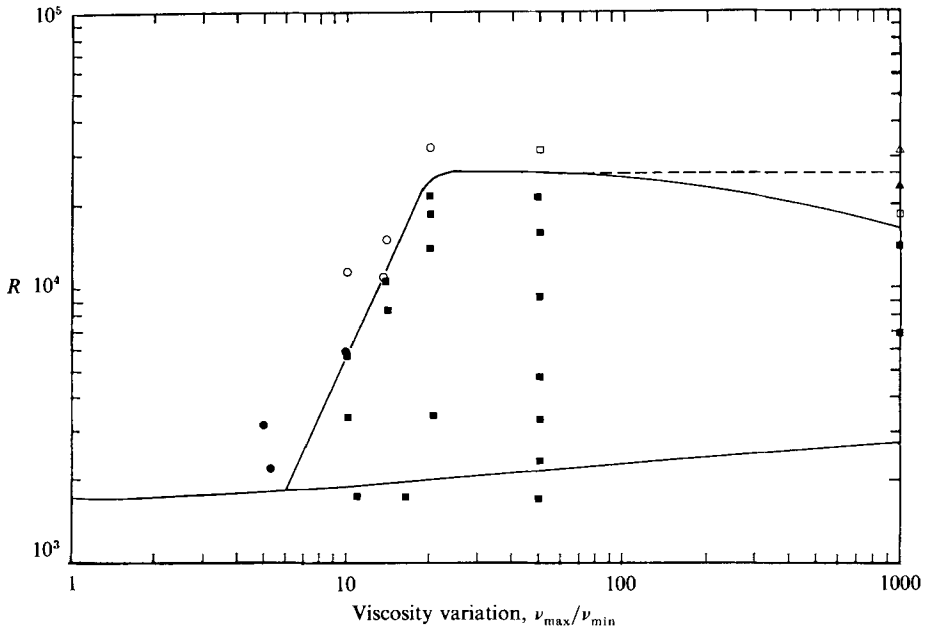

FIGURE 25. The stability map for squares with $k = 3.15$: ■, stable squares; ●, squares broke down into rolls; ○, squares initially broke down into a bimodal pattern; □, squares broke down into a spoke flow. The lower line is the neutral curve for a syrup-type viscosity variation. The dashed line represents the stability of squares if those with a wavenumber at the centre of the stable region at a given viscosity variation (triangular symbols) are considered rather than just those with $k = 3.15$.

8.3. *The stability of hexagons*

At viscosity variations greater than 20 hexagons were observed to be stable up to Rayleigh numbers around 17000 but the transition to other planforms occurred at decreasing Rayleigh numbers as the viscosity variation was reduced below 20 (figure 28). This behaviour is similar to that observed for squares, although the reduction in the Rayleigh number of the transition occurred at a slower rate so that at a viscosity variation of 10 hexagons were stable to higher Rayleigh numbers than squares, a reversal of the situation observed at a viscosity variation of 20. The bottom curve represents the neutral curve and the upper curve was controlled by two main transitions.

8.3.1. *The transition to polygons*

This was seen at Rayleigh numbers just above 17000 and viscosity variations greater than 20, by the methods described in §6. At higher Rayleigh numbers, greater than 25000, the final pattern was the spoke flow.

8.3.2. *The transition to rolls*

This occurred at low Rayleigh numbers and small viscosity variations. As there were three possible directions for the orientation of the roll pattern a completely regular pattern did not form (figure 29). At higher Rayleigh numbers, above R_B, rolls are unstable and the hexagonal pattern broke down into a bimodal flow.

The dashed lines on figure 28 represent the predicted transition of hexagons to rolls from Palm, Ellingsen & Gjevik (1967). The agreement is quite good, unlike the

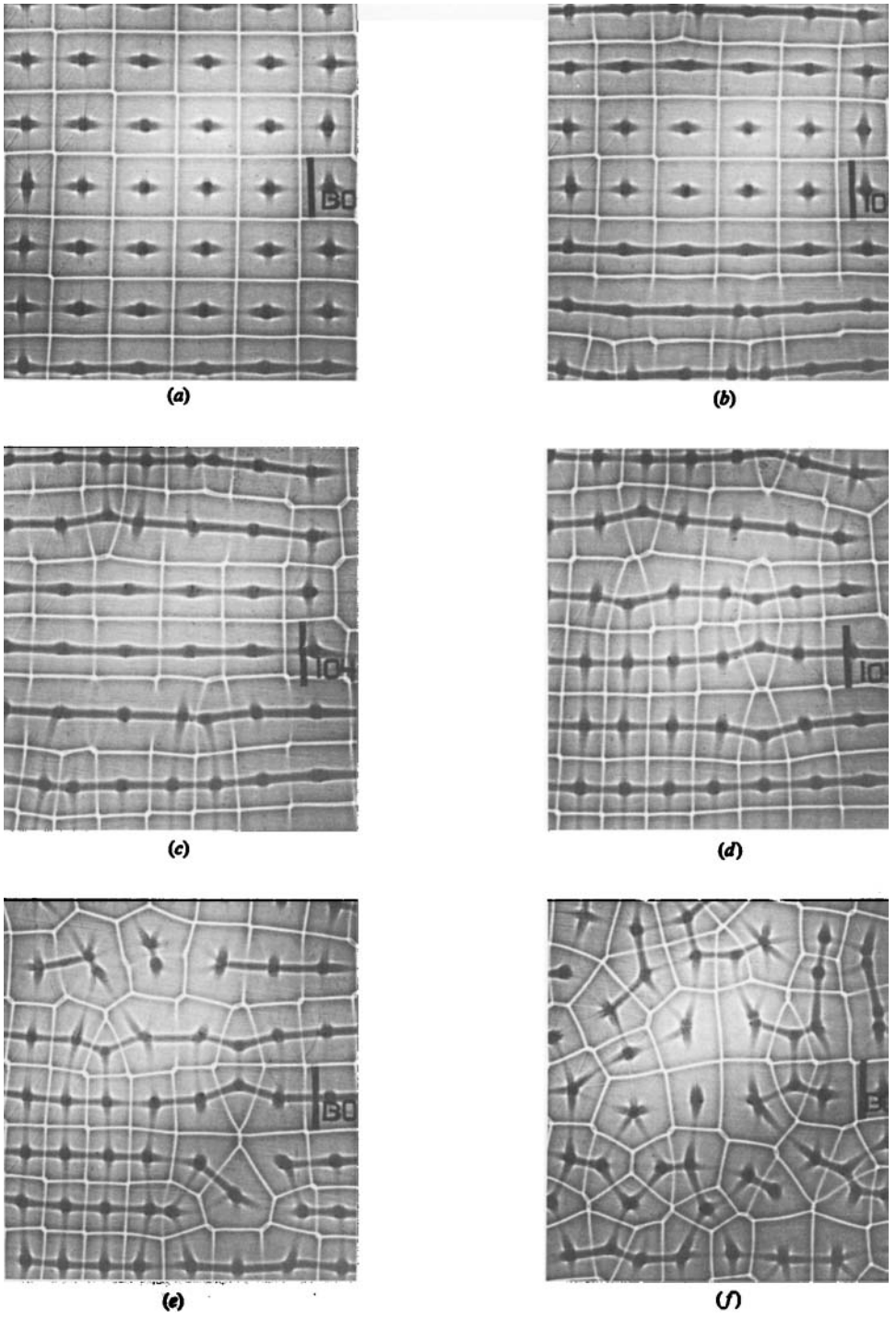

FIGURE 26. The breakdown of squares to a bimodal pattern, which subsequently broke up into a spoke flow, observed in an experiment at a Rayleigh number of 32300 and a viscosity variation of 20.0. (*a*) The rising regions of the cells along the bottom of the screen were observed to join after 2.5 h. (*b*) After 4 h more lines of rising regions had formed and the sinking sheets perpendicular to them died away. (*c*) After 9.75 h new cross-rolls with a larger wavenumber were forming. (*d*) The process was almost completed after 17 h when a nearly uniform bimodal pattern had formed. (*e*) The bimodal pattern was not perfect as there were dislocations in the cross-rolls and the pattern began to break up (27.5 h). (*f*) A spoke-like pattern evolved as the final planform after 44.5 h.

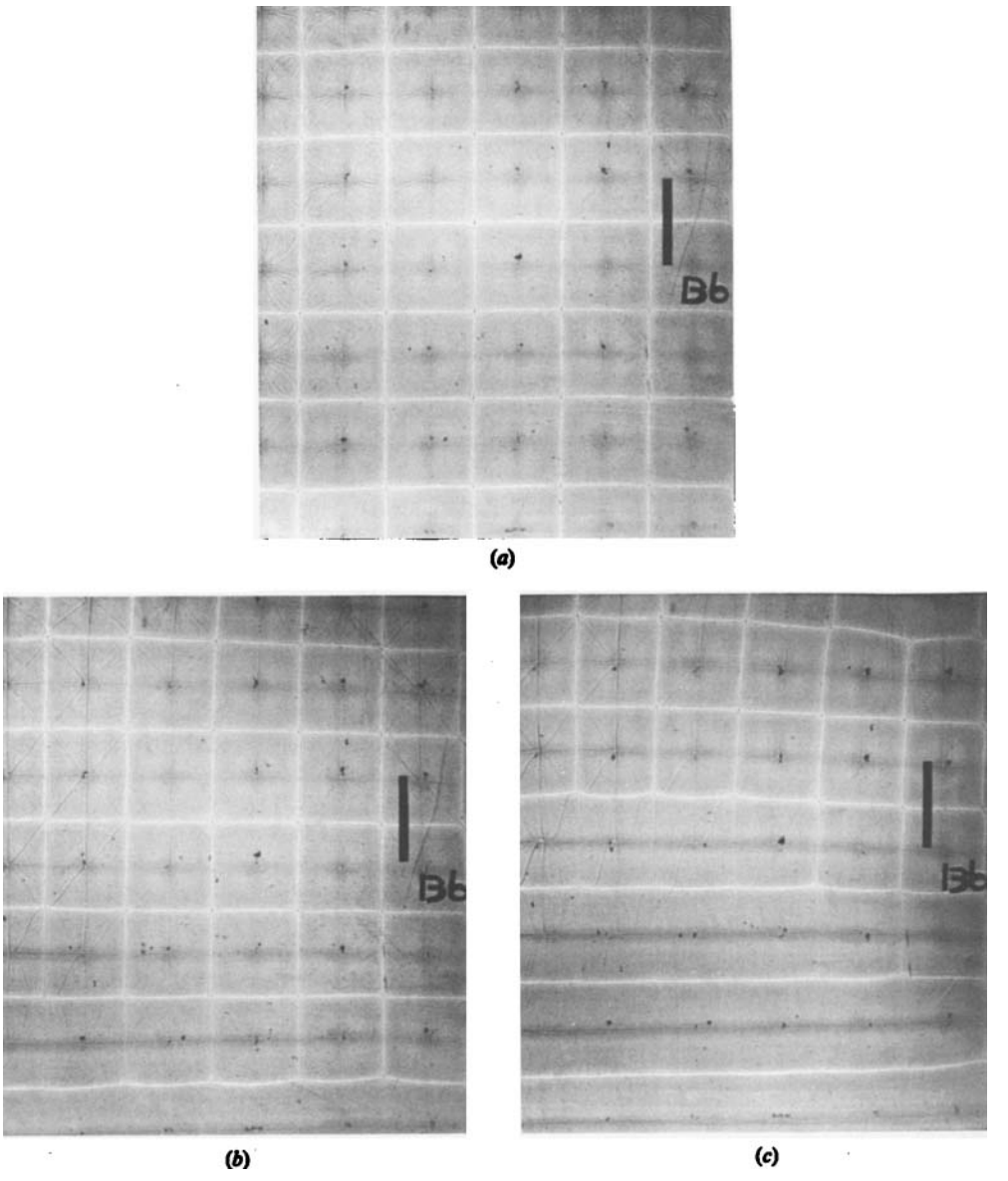

FIGURE 27. Squares with a viscosity variation of 10.1 at a Rayleigh number of 5850 broke down into rolls over a long period of time. (*a*) The initial square pattern after 3.25 h. (*b*) The bottom two rows of squares were transforming into rolls after 23 h. (*c*) Half of the square pattern had broken down into rolls after 48 h.

prediction for the transition of rolls to hexagons, which is surprising as the analysis in both cases assumed a viscosity that varied linearly with temperature.

The stability of rolls, squares and hexagons as a function of R and $\nu_{\max}/\nu_{\min}$ can be summarized in one diagram (figure 30), from which various features of the transitions discussed previously can be understood. Beyond a viscosity variation of 10 the value of R_B drops only slightly and the bimodal pattern produced is unstable to squares. The combined stability map reveals an intersection between boundaries delineating the stability of squares and rolls at a viscosity variation of 10. Any

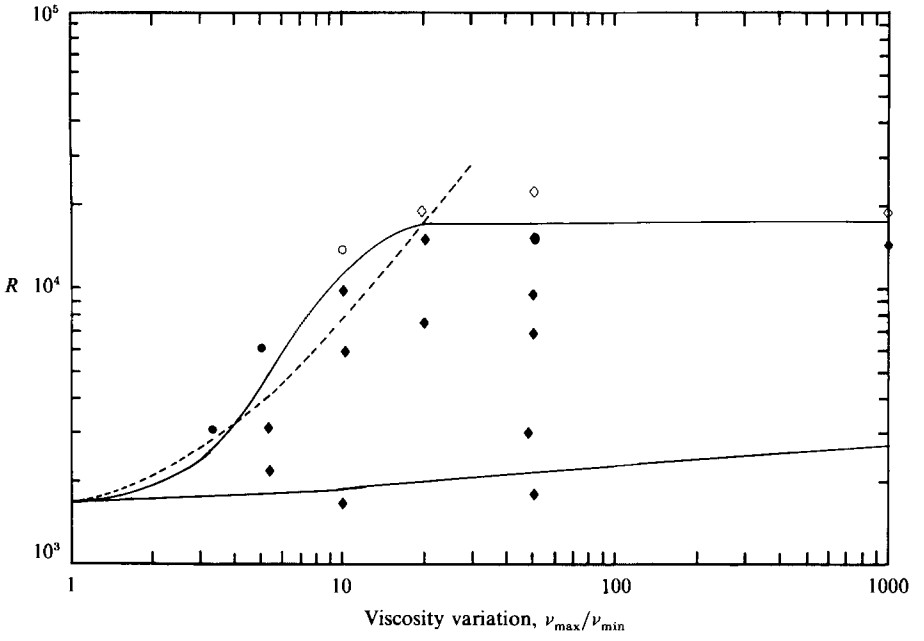

FIGURE 28. The stability map for hexagons with $k = 3.63$: ◆, stable hexagons; ◇, hexagons unstable to polygons; ●, hexagons unstable to rolls; ○, hexagons unstable to a bimodal flow. The lower solid line is the neutral curve for a syrup-type viscosity variation. The dashed curve is the theoretical Rayleigh number of the transition from hexagons to rolls as the Rayleigh number is increased (Palm *et al.* 1967).

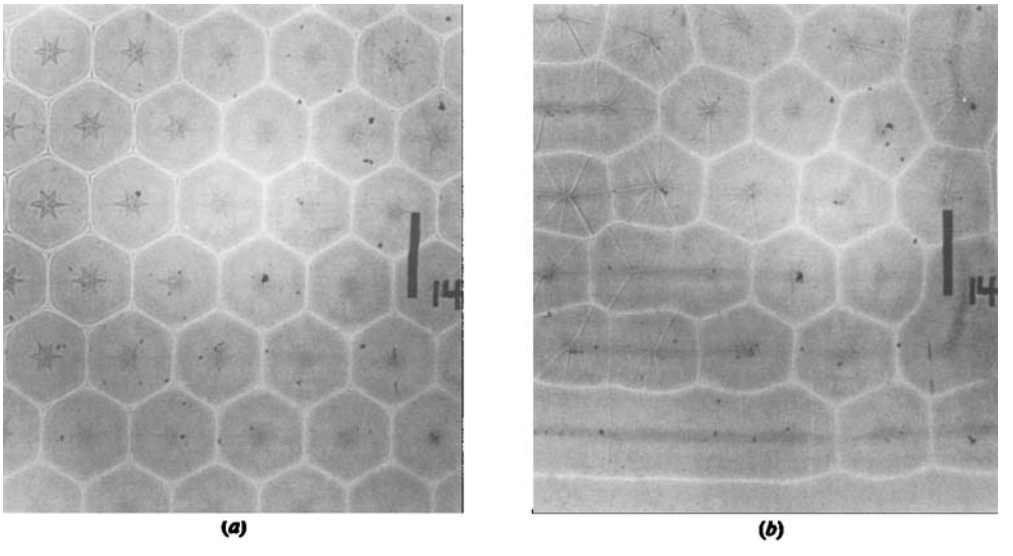

FIGURE 29. An example of the breakdown of hexagons into rolls in an experiment with a viscosity variation of 5.0 and a Rayleigh number of 6100. (*a*) The initial hexagons after 7 h. (*b*) After 36 h rolls were developing in three different orientations.

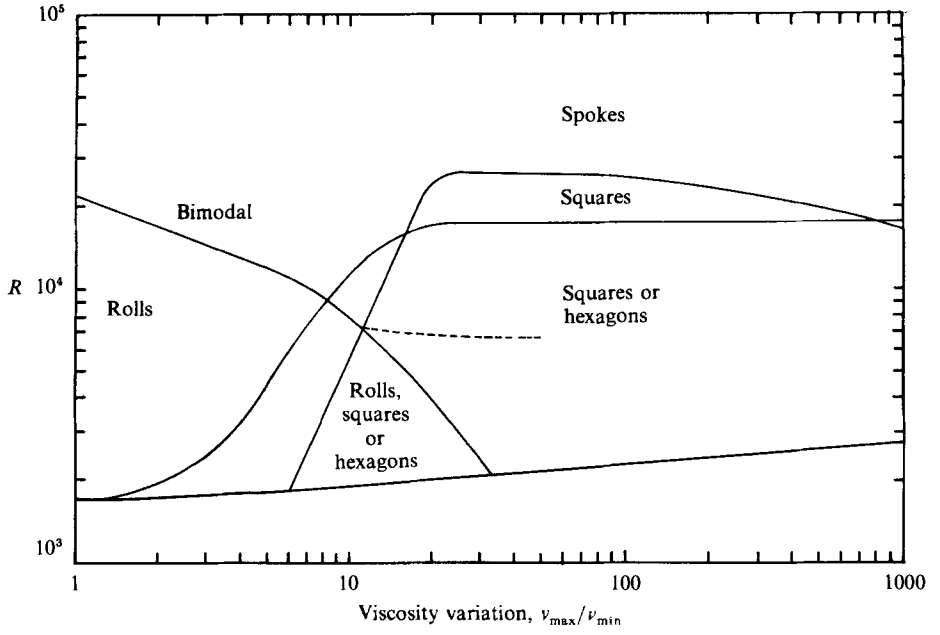

FIGURE 30. A summary of the stability maps for rolls, hexagons and squares with $k = 3.15$. There is a large amount of hysteresis where the realized planform depends on what pattern was originally induced. In one small area rolls, hexagons or squares are all possible planforms. The dashed line represents R_B.

bimodal pattern produced with a Rayleigh number less than 23000 and a viscosity variation greater than 10 was thus in the stable domain or squares and was observed to transform into such a pattern.

In a constant-viscosity fluid the transition of the bimodal pattern to a spoke flow has been observed at Rayleigh numbers, depending on the perfection of the initial pattern, between 70000 and 150000 (Whitehead & Chan 1976). In the variable-viscosity experiments reported above, a bimodal pattern with $R = 30000$ and $\nu_{max}/\nu_{min} = 50$ broke down into a spoke flow and so the Rayleigh number of the bimodal – spoke transition clearly falls from a value of ≈ 100000 at constant viscosity to ≈ 30000 at a viscosity variation of 50. However, this transition was not fully investigated since it was not possible to produce a high Rayleigh number, at a low viscosity variation, with the present apparatus and fluid.

The stability map produced by Oliver & Booker (1983) shows that the transition between hexagons and squares occurs at a Rayleigh number of ≈ 2500 for a flow with a viscosity variation of 50. This behaviour was not observed in the experiments carried out above. The experimental procedure used by Oliver & Booker was to raise the Rayleigh number in increments of 100 with 4 h between adjustments ($d^2/\kappa = 24$ min). Their small circular experimental apparatus did not allow the initiation of a regular hexagonal pattern so they could only study the evolution of the semiregular hexagons, produced at R_c from random initial conditions. In a similar experiment using the above apparatus and hexagons formed from random initial conditions, the transition to squares was not observed as the Rayleigh number was incremented slowly from 1800 to 4500 over a period of two weeks. This disagreement with Oliver & Booker would suggest that the circular boundaries of their apparatus had a large effect on the planform selected by the layer.

One particularly interesting feature of the combined diagram (figure 30) is that it reveals a small region in which squares, rolls and hexagons are all stable, the actual planform depending upon the initial pattern. The change between constant- and strongly variable-viscosity behaviour is seen to occur between a viscosity variation of 10 and 20.

I wish to thank Dan McKenzie for suggesting this topic, which formed the research for my Ph.D., and for many helpful discussions. Thanks also go to Frank Richter for his useful comments and the use of his data in figure 22. I am also very grateful to Tate & Lyle for their generous donations of Lyle's Golden Syrup. This work forms part of a continuing investigation of mantle convection funded by the Natural Environment Research Council. Earth Sciences Contribution Number 1063.

REFERENCES

BOOKER, J. R. 1976 Thermal convection with strongly temperature-dependent viscosity. *J. Fluid Mech.* **76**, 741–754.

BUSSE, F. H. 1967*a* On the stability of two-dimensional convection in a layer heated from below. *J. Math. Phys.* **46**, 140–149.

BUSSE, F. H. 1967*b* The stability of finite amplitude cellular convection and its relation to an extremum principle. *J. Fluid Mech.* **30**, 625–649.

BUSSE, F. H. & FRICK, H. 1985 Square-pattern convection in fluids with strongly temperature-dependent viscosity. *J. Fluid Mech.* **150**, 451–465.

BUSSE, F. H. & RIAHI, N. 1980 Non-linear convection in a layer with nearly insulating boundaries. *J. Fluid Mech.* **96**, 243–256.

BUSSE, F. H. & WHITEHEAD, J. A. 1971 Instabilities of convection rolls in a high Prandtl number fluid. *J. Fluid Mech.* **47**, 305–320.

CHANDRASEKHAR, S. 1961 *Hydrodynamic and Hydromagnetic Stability.* Clarendon.

CHEN, M. M. & WHITEHEAD, J. A. 1968 Evolution of two-dimensional periodic Rayleigh convection cells of arbitrary wavenumbers. *J. Fluid Mech.* **31**, 1–15.

HOARD, C. O., ROBERTSON, C. R. & ACRIVOS, A. 1970 Experiments on cellular structure in Bénard convection. *Intl. J. Heat Mass Transfer* **13**, 849.

KRISHNAMURTI, R. 1968 Finite amplitude convection with changing mean temperature. Part 1. Theory. *J. Fluid Mech.* **33**, 445–455.

OLIVER, D. S. & BOOKER, J. R. 1983 Planform and heat transport of convection with strongly temperature dependent viscosity. *Geophys. Astrophys. Fluid Dyn.* **27**, 73–850.

PALM, E. 1960 On the tendency towards hexagonal cells in steady convection. *J. Fluid Mech.* **8**, 183–192.

PALM, E., ELLINGSEN, T. & GJEVIK, B. 1967 On the occurrence of cellular motion in Bénard convection. *J. Fluid Mech.* **30**, 651–661.

PROCTOR, M. R. E. 1981 Planform selection by finite amplitude thermal convection between poorly conducting slabs. *J. Fluid Mech.* **113**, 469–485.

RAYLEIGH, LORD 1916 On convection currents in a horizontal layer of fluid when the higher temperature is on the underside. *Phil. Mag.* (6) **32**, 529.

RICHTER, F. M. 1978 Experiments on the stability of convection rolls in fluids whose viscosity depends on temperature. *J. Fluid Mech.* **89**, 553–560.

RICHTER, F. M., NATAF, H.-C. & DALEY, S. F. 1983 Heat transfer and horizontally averaged temperature of convection with large viscosity variations. *J. Fluid Mech.* **129**, 173–192.

SOMERSCALES, E. F. C. & DOUGHERTY, T. S. 1970 Observed flow patterns at the initiation of convection in a horizontal liquid heated from below. *J. Fluid Mech.* **42**, 755–768.

STENGEL, K. C., OLIVER, D. S. & BOOKER, J. R. 1982 Onset of convection in a variable viscosity fluid. *J. Fluid Mech.* **120**, 411–431.

WHITE, D. B. 1981 Experiments with convection in a variable viscosity fluid. Ph.D. thesis, University of Cambridge.

WHITEHEAD, J. A. & CHAN, G. L. 1978 Stability of Rayleigh–Bénard convection rolls and bimodal flow at moderate Prandtl numbers. *Dyn. Atmos. Oceans* **1**, 33–49.

WHITEHEAD, J. A. & PARSONS, B. 1978 Observations of convection at Rayleigh numbers up to 760,000 in a fluid with a large Prandtl number. *Geophys. Astrophys. Fluid Dyn.* **19**, 201–217.

WRAY, F. 1978 Some convective flows of geophysical interest. Ph.D. thesis, University of Cambridge.